Spontaneous human CD8 T cell and EAE-inducible human CD4/CD8 T cell lesions in the brain and spinal cord of HLA-DRB1*15-positive MS PBMC humanized mice

Irini Papazian[1], Maria Kourouvani[1,2], Anastasia Dagkonaki[1], Vasileios Gouzouasis[1,3], Lila Dimitrakopoulou[4], Nikolaos Markoglou[5], Fotis Badounas[1,6], Theodore Tselios[7], Maria Anagnostouli[5], Lesley Probert[1,8]

1. Laboratory of Molecular Genetics, Department of Immunology, Hellenic Pasteur Institute, Athens, Greece.
2. Athens International Master's Programme in Neurosciences, Department of Biology, National and Kapodistrian University of Athens, Athens, Greece.
3. Department of Molecular Biology and Genetics, Democritus University of Thrace, Alexandroupolis, Greece.
4. Department of Hematology, Laiko General Hospital, National and Kapodistrian University of Athens, Athens, Greece.
5. Multiple Sclerosis and Demyelinating Diseases Unit, First Department of Neurology, School of Medicine, National and Kapodistrian University of Athens, NKUA, Aeginition University Hospital, Athens, Greece.
6. Transgenic Technology Unit, Hellenic Pasteur Institute, Athens, Greece.
7. Department of Chemistry, University of Patras, Rio, Patras, Greece.

Keywords: Humanized mice, peripheral blood mononuclear cells, HLA-DRB1*15 MS risk factor, multiple sclerosis, experimental autoimmune encephalomyelitis, natalizumab, Epstein-Barr virus infection status

8. Correspondence: Lesley Probert; lesley.probert@gmail.com, lesley@pasteur.gr

Summary

Autoimmune diseases of the central nervous system (CNS) such as multiple sclerosis (MS) are only partially represented in current experimental models and the development of humanized immune mice is crucial for better understanding of immunopathogenesis and testing of therapeutics. We describe a humanized mouse model with several key features of MS. Severely immunodeficient B2m-NOG mice were transplanted with peripheral blood mononuclear cells (PBMC) from HLA-DRB1-typed MS and healthy (HI) donors and showed rapid engraftment by human T and B lymphocytes. Mice that received cells from MS patients with recent/ongoing Epstein-Barr virus (EBV) reactivation, determined by the presence of plasma anti-EBV antibodies, showed high B cell engraftment capacity. Both HLA-DRB1*15 (DR15) MS and DR15 HI mice, not HLA-DRB1*13 (DR13) MS mice, developed human T cell infiltration of CNS borders and parenchyma. DR15 MS mice uniquely developed inflammatory lesions in brain and spinal cord grey matter, with spontaneous, hCD8 T cell lesions in non-immunized mice, and mixed hCD8/hCD4 T cell lesions in EAE immunized mice, with variation in localization and severity between different patient donors. Main limitations with this model for further development are poor monocyte engraftment and lack of demyelination, lymph node organization and IgG responses. These results show that PBMC humanized mice represent promising research tools for investigating MS immunopathology in a patient-specific approach.

Introduction

Multiple sclerosis (MS) is a complex chronic inflammatory demyelinating and neurodegenerative disease of the central nervous system (CNS) with autoimmune characteristics. Pathological hallmarks are focal plaques of immune-mediated demyelination in the white matter, inflammation at CNS borders and diffuse demyelination and neurodegeneration of the grey and white matter of the brain and spinal cord. Genome wide association studies show that the vast majority of MS risk genes are related to immune activation and function, thereby strongly supporting the role of adaptive immunity in MS pathogenesis. These include the strongest MS associated genetic risk factor, human leukocyte antigen (HLA) DRB1*15 haplotype, encoded by two DRB* genes, *DRB1*15:01* (DR2b) and *DRB5*01:01* (DR2a), of the MHC class II (MHCII) that restricts $CD4^+$ T cells (1,2). Pathological analyses of autopsy tissues reveal $CD8^+$ lymphocytes and monocytes as the main CNS infiltrating cells, with B cells accumulating in meningeal and perivascular spaces, and relatively few infiltrating $CD4^+$ T cells (3). Studies in animal models, mainly experimental autoimmune encephalomyelitis (EAE), showing that myelin-reactive T cells are necessary for EAE induction, as well as the effectiveness of current immunotherapies in MS patients that work mainly by targeting peripheral immune responses, further support an autoimmune pathogenesis for MS.

EAE and MS share many clinical, immunological, and pathological similarities (4,5), but they also present significant differences (6,7). One difference is the predominance of $CD8^+$ T cells in MS lesions, while these cells are scarce in the CNS of EAE mice (8). In addition, the inflammatory process in EAE primarily targets the spinal cord, whereas in MS it also targets the brain. Moreover, while some MS drugs were discovered from research in the EAE model (natalizumab, glatiramer acetate), there is a relatively low or moderate success rate of drugs that showed high efficacy in both the EAE model and the human disease (9). These differences infer that different pathways or mechanisms are prevalent in MS versus EAE (10,11). Differences are further highlighted by recent clinical data showing the critical importance of B cells to MS pathology, a cell population that does not show important functional participation in most EAE models (12,13). The development of animal models capable of developing human immune system is crucial to the study of human immune-mediated diseases such as MS, and for evaluating the safety and efficacy of human immunotherapies. Most current studies with humanized mouse models use immunodeficient non-obese diabetic (NOD) - severe combined immunodeficiency disorder (*scid*) mice deficient or mutant for the common cytokine receptor γ-chain gene (*IL2rg)* (named NSG or NOG mice, respectively) that lack B, T cells and NK cells and have defective innate immune responses (14–17). These mouse strains readily engraft with human peripheral blood mononuclear cells (PBMC) without prior irradiation, as murine MHC molecules support the proliferation of both human $CD4^+$ and $CD8^+$ T cells, with $CD8^+$ T cells predominating. Recent variants of these strains lacking MHC class I molecules (B2m) show increased CD4 to CD8 ratios and a longer time window before onset of xenogeneic graft versus host disease (GVHD) and represent improved strains for the study of human immune responses (18,19). Previous studies showed that PBMC humanized NSG mice with cells from healthy donors are susceptible to EAE, exhibiting subclinical disease, with infiltration of the brain and spinal cord by $CD4^+$ and $CD8^+$ T cells, but not monocytes (20).

To investigate the potential of PBMC from MS patients to induce CNS-directed immunopathology in humanized mice, we engrafted B2m-NOD/*scid*-IL2Rγ^{null} (B2m-NOG) mice with PBMC from human donors based on HLA-DRB1 genotype, RRMS diagnosis and therapy, and monitored CNS inflammation that developed spontaneously or after immunization for EAE with myelin antigens. We show that PBMC from MS and healthy (HI) donors rapidly engraft B2m-NOG mice with human (h)CD4$^+$ and hCD8$^+$ T cells and B cells, with donor-specific differences towards proportions of human immune cell populations engrafted and propensity to develop CNS inflammation. Mice transplanted with PBMC from HLA-DRB1*15-positive (DR15) MS patients uniquely developed spontaneous hCD8$^+$ T cell lesions in the spinal cord grey matter and brainstem, and prominent brain white and grey matter lesions with mixed hCD4/hCD8 T cells in mice immunized with myelin peptides. Our results show that PBMC humanized B2m-NOG mice partially reproduce MS immunopathology and can be used to investigate human immune responses towards CNS in a simple, rapid, and personalized manner.

Results

Reconstitution of human adaptive immune system in B2m-NOG mice engrafted with PBMC from MS patient and HI donors

Six long-term RRMS patients, of which five were HLA-DRB1*15-positive (DR15 MS1-5) and one HLA-DRB1*13-positive (DR13 MS), all presenting with highly active disease following immunomodulatory treatment with natalizumab, were selected as PBMC donors (Table 1). A DR15-positive healthy individual (DR15 HI) was selected as a control donor. Fresh blood samples were used for immunoprofiling by flow cytometry with a panel of standard human immune cell marker antibodies (Supplementary Table 1A, B), for screening of plasma antibody responses to viruses (Table 1; and Supplementary Table 1C for clinical interpretation of Epstein-Barr virus/EBV results), and for the isolation of fresh PBMC. Groups of 7-8 B2m-NOG mice were injected intravenously with freshly prepared PBMC (1 x 10^7/mouse) from each donor (Supplementary Table 2, protocol 1). The transplanted mice were monitored for human immune cell engraftment by flow cytometry analysis of small blood samples recovered from the tail vein at different time points and all showed progressive engraftment by human CD45$^+$ (hCD45$^+$) leukocytes from day 7 (Fig. 1A; Supplementary Fig. 1). At day 14 post-transplantation (dpt 14), 4-5 mice from each group were immunized for EAE using a mixture of immunodominant T cell myelin peptide antigens, following two different protocols. In EAE experiment 1, groups of DR13 MS, DR15 MS1 and DR15 HI mice were immunized twice, 7 days apart, using 200 µg each peptide/mouse, each time. In EAE experiment 2, groups of DR15 MS2-5 were immunized once, using 100 µg each peptide/mouse. Several PBMC donors used in this study were previously shown to have human T cell proliferation responses to myelin peptides (21) (Table 1). Non-immunized mice, and mice immunized for EAE with low-dose peptides (1x100 µg) showed steadily increasing levels of blood hCD45$^+$ leukocytes up to sacrifice at dpt 42 (Fig. 1A; Supplementary Fig. 1). Mice immunized for EAE with high-dose peptides (2x200 µg) showed reduced levels of blood hCD45$^+$ leukocytes following immunization (Fig. 1A). Further FACS analysis showed preferential expansion of hCD4$^+$ T lymphocytes compared to hCD8$^+$ T lymphocytes in blood and spleens of all engrafted mice (Fig. 1B, C; Supplementary Fig. 1), a finding consistent with a previous report describing the B2m-NSG model (18).

142 Successful engraftment of mice by hCD45$^+$ leukocytes was confirmed in the spleen recovered
143 from non-immunized and immunized mice at sacrifice on dpt 42. Further analysis of
144 splenocytes revealed robust engraftment of hCD4$^+$ and hCD8$^+$ T cells in all mice, and of hCD19$^+$
145 B cells in DR13 MS, DR15 MS3 and DR15 MS5 mice (Fig. 1C; Supplementary Table 3). Notably,
146 B cell engraftment was best in MS patients interpreted as having suspect recent or ongoing
147 reactivation of EBV, as determined by plasma levels anti-EBV antibodies (Table 1;
148 Supplementary Table 1C). Human immune cells other than T and B cells, notably monocytes,
149 were undetectable in dpt 42 spleen. Analysis of cytokine production by intracellular staining
150 showed high proportions of IFN-γ-producing hCD4$^+$ and hCD8$^+$ splenocytes, and IL-17A-
151 producing hCD4$^+$ and hCD4$^-$ splenocytes in both immunized and non-immunized mice (Fig.
152 1D).
153
154 To estimate the contribution of mouse myeloid cell populations in the humanized mice, we
155 analyzed peripheral blood from naïve B2m-NOG mice, and from naïve and CFA-immunized
156 (day 8 post-immunization) NOD-*scid* parental strain and wild-type C57BL/6 (B6) mice, by flow
157 cytometry. Immature Ly6C^{hi} monocytes and Ly6G$^+$ cells are known to massively expand in the
158 periphery of B6 mice following immunization with adjuvants and are critical for the
159 development of EAE (22,23). Unlike B6 mice, very high proportions of mouse (m) CD11b$^+$,
160 mCD11b$^+$Ly6C^{hi} and mCD11b$^+$Ly6G$^+$ myeloid cells were already present in the blood of naive
161 B2m-NOG and NOD-*scid* mice, and were not significantly increased by immunization
162 (Supplementary Table 4).
163
164 Functionality of the human immune system in B2m-NOG mice was investigated using an *ex*
165 *vivo* proliferation assay for T cell responses in splenocytes (23), and a cell-based assay for anti-
166 MOG antibody responses in plasma. Briefly, splenocytes recovered from non-immunized and
167 immunized mice at sacrifice were stimulated *ex vivo* individually with the 4 myelin peptides
168 used for immunization (mMOG35-55, hMOG35-55, MOG1-20, MBP83-99). T cell proliferation
169 responses were measured using a CFSE dilution assay. Splenocytes isolated from DR13 MS
170 mice (Fig. 1E), showed significant T cell proliferation responses to all myelin peptides, equal
171 to control splenocytes stimulated with anti-hCD3 antibody. Notably, splenocytes from DR15
172 MS and DR15 HI mice showed limited or absence of T cell proliferation responses to myelin
173 peptides or polyclonal T cell stimuli, anti-hCD3 antibody and phytohemaglutinin (PHA)
174 (Supplementary Fig. 1). The difference in responses between DR13 and DR15 donors cannot
175 be explained by differences in human B cell engraftment, which are potential antigen-
176 presenting cells in the *ex vivo* T cell proliferation assay, because B cell engraftment was seen
177 in DR13 MS and DR15 MS mice (Fig. 1C). A previous study showed that T cells isolated from
178 DR15 MS patients display high levels of autoproliferation (24). Therefore, it is possible that
179 poor human T cell proliferation responses in DR15 mice might result from inherently high T
180 cell autoproliferation in the DR15 MS donor PBMC prior to engraftment, although this
181 possibility needs to be formally tested. Alternatively, CD4+ T cells may become nonresponsive
182 to anti-CD3 antibody once engrafted into B2m-NOG mice, as previously reported in NOD-scid
183 mice (25). Anti-hMOG IgG antibody responses were not detectable in the plasma of any mice
184 at any time point.
185
186 We next investigated whether draining lymph nodes (LN) structures could be identified in the
187 immunized mice at sacrifice. Mice lacking the common cytokine receptor γ-chain gene are
188 known to have poor lymphoid organ structure and functioning, because NK cells are needed

189 for the formation of LN inducer cells, which in turn are needed for LN organogenesis (26).
190 Nevertheless, the inguinal fat tissue from several immunized mice showed accumulated
191 masses of leukocytes containing mCD45- and hCD45-positive leukocytes, CD8-, CD4- and
192 CD20-positive lymphocytes by immunohistochemistry, although lacking obvious LN
193 organization (Fig. 1F). Together the results show that human T and B lymphocytes are
194 efficiently engrafted in B2m-NOG mice by PBMC from MS patients, that functional T cell
195 responses can be detected depending upon the PBMC donor, while lack of organized LN and
196 germinal centers prevents the generation of anti-MOG IgG antibody responses.
197
198 *Human T cells accumulate at CNS borders in non-immunized DR15 MS and DR15 HI mice, and*
199 *form spontaneous parenchymal lesions in brain and spinal cord of DR15 MS mice*
200 For the period of the study, none of the engrafted mice showed clinical symptoms of
201 neuroinflammation or EAE using criteria commonly used for scoring EAE (21), or other
202 neurological deficits (27). Mild symptoms of GVHD, specifically fur ruffling and reduced
203 mobility (28), were recorded in few mice independent of group close to the time of sacrifice.
204 To determine whether human immune cells enter CNS tissues in PBMC humanized B2m-NOG
205 mice, we performed immunohistochemical analyses of serial sections from brain and spinal
206 cord recovered from non-immunized mice at sacrifice using marker antibodies for human and
207 mouse immune cells as well as for mouse microglia and astrocytes. To further monitor GVHD
208 development we also performed standard histological analyses of lung and liver, two main
209 tissue targets of GVHD.
210
211 DR13 MS humanized mice showed very few hCD45-positive leukocytes at CNS borders,
212 specifically meninges, and none in CNS parenchyma, and no further analysis was made (data
213 not shown). DR15 HI mice showed an accumulation of human immune cells at CNS borders,
214 particularly the meninges and some in the choroid plexus of the interventricular foramen
215 between lateral and third ventricles of the brain, and few cells scattered throughout the brain
216 parenchyma (Fig. 2A-C). Both brain border and parenchymal hCD45-positive immune cells
217 comprised mainly hCD8-positive T cells (Fig. 2D), leading to low hCD4/hCD8 T cell ratios,
218 especially in parenchyma (Fig. 2E). Mild activation of Iba1-positive microglia and GFAP-
219 positive astrocytes was seen at sites of immune cell accumulation at CNS borders (Fig. 2C). In
220 spinal cord, hCD3-positive T cells accumulated at borders and few individual cells infiltrated
221 parenchyma of white and grey matter (Fig. 3A-C), forming rare small T cell lesions (≥ 3
222 adjacent cells) in the white matter (Fig. 3A, bottom left panel, arrowhead). Spinal cord-
223 infiltrating cells in DR15 HI mice also comprised mainly hCD8-positive T cells, leading to low
224 hCD4/hCD8 T cell ratios (Fig. 3D). Mouse CD45-positive cells were rare at barriers, absent
225 from parenchyma, and demyelination was not observed in the brain or spinal cord of DR15 HI
226 mice.
227
228 Three of the five groups of DR15 MS mice, specifically DR15 MS1, DR15 MS3 and DR15 MS5
229 mice, showed severe spontaneous CNS pathology with accumulation of human immune cells
230 at borders, particularly the meninges and choroid plexus of the interventricular foramen
231 between lateral and third ventricles, widespread immune cell infiltration of the parenchyma,
232 and T cell lesions in the brain, brainstem and spinal cord. Brain border and parenchymal
233 hCD45-positive immune cells comprised mainly hCD8-positive T cells (Fig. 2A-D), leading to
234 low hCD4/hCD8 T cell ratios, especially in the parenchyma (Fig. 2E). These mice showed
235 numerous spontaneous parenchymal hCD45-positive cell lesions (≥ 3 adjacent cells). The

236 location and severity of parenchymal lesions were different in each patient, and involved
237 brainstem (DR15 MS1; Fig. 2F), hippocampus (DR15 MS3; Fig. 2Gi, ii), optic chiasm (DR15 MS3;
238 Fig. 2H), and sub-hippocampal regions (DR15 MS3; Fig. 2Giii, DR15 MS5; Fig. 2I, J). Locally
239 activated Iba1-positive microglia and GFAP-positive astrocytes were observed at sites of
240 immune cell accumulation (Fig. 2C). DR15 MS2 and DR15 MS4 mice showed only few human
241 immune cells at borders and no parenchymal lesions. In the spinal cord, hCD3-positive T cells
242 accumulated at borders and infiltrated both white and grey matter parenchyma, forming
243 lesions in both areas (Fig. 3A right panels, arrowheads). Numbers of parenchymal hCD3-
244 positive T cells counted in whole spinal cord sections tended to be increased in DR15 MS1
245 mice compared to control HI mice (Fig. 3B), and numbers of T cell lesions in the grey matter
246 were significantly increased (Fig. 3C). Unlike control HI mice, DR15 MS1 mice showed
247 numerous small T cell lesions in the grey matter, often close to the central canal suggesting
248 this is a main site of human T cell entry into the spinal cord grey matter (Fig. 3A, top right
249 panel, arrowheads). Spinal cord-infiltrating immune cells in DR15 MS1 mice also comprised
250 mainly hCD8-positive T cells, leading to low hCD4/hCD8 T cell ratios (Fig. 3D). In contrast to
251 hCD45-positive immune cells that were scattered in spinal cord parenchyma (Fig. 3E), mouse
252 CD45-positive cells were rare at barriers, absent from parenchyma, and demyelination was
253 not observed in the brain or spinal cord of any DR15 MS mice.
254
255 To determine whether differences in the severity of CNS immune infiltration in the immunized
256 mice was secondary to levels of GVHD inflammation in the periphery, we performed semi-
257 quantitative analysis of H&E stained liver and lung sections, which are main targets of GVHD
258 responses (28). The mouse groups showed equal levels of inflammation in both liver and lung,
259 revealing a dissociation between peripheral GVHD and CNS inflammation (Supplementary Fig
260 2). These results show that non-immunized DR15 MS1 humanized mice show increased
261 infiltration of brain and spinal cord by human T cells compared to non-immunized DR15 HI
262 mice, and uniquely develop spontaneous T cell lesions in spinal cord grey matter and brain
263 parenchyma.
264
265 *Immunization with myelin peptides increases hCD4 T cell infiltration of CNS parenchyma*
266 *resulting in mixed hCD4/hCD8 T cell lesions in brain and spinal cord of DR15 MS and DR15 HI*
267 *mice*
268 To further investigate whether human immune cells have the potential to induce CNS
269 immunopathology in PBMC humanized B2m-NOG mice, we immunized mice for EAE. In a
270 previous study, humanized HLA-DR2b transgenic mice lacking all mouse MHCII genes were
271 found to require high amounts of peptide antigen than B6 mice to induce clinical EAE (21).
272 Here, EAE tests in wild-type B6 mice showed that disease could be induced by immunization
273 with high amounts of peptides with no evidence of increased morbidity or mortality
274 (Supplementary Fig. 3A, B). A peptide cocktail containing myelin epitopes previously
275 associated with MS, specifically hMOG35-55, MOG 1-20 and MBP83-99 (29–32), plus
276 mMOG35-55, was chosen for immunization of groups of 12-14-week-old humanized B2m-
277 NOG mice on dpt 14. In the first experiment, groups of B2m-NOG mice engrafted with PBMC
278 from DR13 MS, DR15 MS1 and DR15 HI donors received a double immunization with 200
279 µg/peptide spaced 7 days apart, similar to that used in HLA-DR2b transgenic mice. In the
280 second experiment, groups of B2m-NOG mice engrafted with PBMC from DR15 MS2-5 donors
281 received a single immunization with 100 µg/peptide, to reduce the possibility of T cell
282 tolerance (Supplementary Fig. 3C). None of the PBMC humanized B2m-NOG mice immunized

283 with myelin antigens developed typical clinical symptoms of EAE, a finding consistent with a
284 previous study in NSG mice humanized with PBMC from healthy donors (20).
285
286 To investigate whether immunization for EAE increased immune cell infiltration of the brain
287 and spinal cord we performed immunohistochemical analysis of tissues recovered from the
288 mice at sacrifice at dpt 42. Immunized DR13 MS mice and their non-immunized controls
289 showed very few hCD45-positive leukocytes at CNS borders and infiltrating spinal cord
290 parenchyma, so no further analysis was made (data not shown). Immunized DR15 HI mice
291 showed accumulation of hCD45-positive leukocytes at the borders, particularly the meninges
292 and choroid plexus, and few cells scattered throughout the parenchyma (Fig. 4A-C). Brain
293 border and parenchymal human immune cells comprised hCD8-positive T cells, and in
294 contrast to non-immunized controls also contained high numbers of hCD4-positive cells (Fig.
295 4D), leading to high hCD4/hCD8 T cell ratios (Fig. 4E). This finding is consistent with successful
296 activation of hCD4-positive T cells by the EAE immunization protocol. In one of five immunized
297 DR15 HI mice, a small T cell lesion was detected in the optic tract (Fig. 4B, arrowhead). Locally
298 activated Iba1-positive microglia and GFAP-positive astrocytes were present at sites of
299 immune cell accumulation at borders and in optic tract lesions (data not shown). In spinal
300 cord, hCD3-positive T cells accumulated at borders and individual cells infiltrated parenchyma
301 of grey and white matter (Fig. 5A, B), forming small T cell lesions in the white matter (Fig. 5A,
302 bottom left panel, arrowhead, C). In the spinal cord of immunized DR15 HI mice, border and
303 parenchymal T cells comprised hCD8-positive T cells and also higher numbers of hCD4-
304 positive T cells compared to non-immunized controls, leading to higher hCD4/hCD8 T cell
305 ratios (Fig. 5D). Mouse CD45-positive cells were rare at barriers, absent from parenchyma,
306 and demyelination was not observed in the brain or spinal cord of immunized DR15 HI mice.
307
308 Immunized DR15 MS1-5 mice generally showed prominent accumulation of human immune
309 cells at CNS borders, widespread immune cell infiltration of the parenchyma and
310 development of T cell lesions in the brain and the spinal cord. Brain border and parenchymal
311 hCD45-positive leukocytes comprised hCD8-positive T cells together with higher numbers of
312 hCD4-positive cells compared to non-immunized controls (Fig. 4C, D), leading to higher
313 hCD4/hCD8 T cell ratios (Fig. 4E). Border and parenchymal T cells were generally increased in
314 immunized DR15 MS mice compared to immunized DR15 HI mice, but differences did not
315 reach significant due to intra-group variation (Fig. 4D). Unique features of immunized DR15
316 MS mice included large human immune cell lesions in the corpus callosum white matter of
317 DR15 MS1 mice containing both hCD8- and hCD4-positive T cells (Fig. 4A, F), without
318 detectable myelin damage (Fig. 4F inset, G), a white matter lesion in DR15 MS2 mice (Fig. 4A,
319 H), numerous white and grey matter lesions in DR15 MS3 mice (Fig. 4A, I, J), and small sub
320 thalamic grey matter lesions in DR15 MS5 mice (Fig. 4A, K). Increased brain infiltration by CD4-
321 positive T cells in immunized mice was not associated with increased frequency of brain
322 lesions, but rather the presence of mixed lesions containing both CD4- and CD8-postive T cells
323 (Fig. 4J). Correlation analysis showed a positive correlation between numbers of hCD4 and
324 hCD8 with numbers of hCD45 lesions (Fig. 4L). Locally activated Iba1-positive microglia and
325 GFAP-positive astrocytes were present at sites of human immune cell entry at CNS borders
326 and in T cell lesions (Fig. 4F, and data not shown). In spinal cord, hCD3-positive T cells
327 accumulated at borders and individual cells infiltrated parenchyma of grey and white matter
328 (Fig. 5A, B), forming small T cell lesions only in the white matter (WM) (Fig. 5A, right panels;
329 Cii). Numbers of parenchymal hCD3-positive T cells counted in whole spinal cord sections, and

330 numbers of T cell lesions in the white matter were equal to those in immunized HLA-DR15 HI
331 mice (Fig. 5B). Spinal cord border and parenchymal T cells of immunized DR15 MS1 mice
332 comprised hCD8-positive T cells and also high numbers of hCD4-positive T cells compared to
333 non-immunized controls, leading to higher hCD4/hCD8 T cell ratios (Fig. 5D). Mouse CD45-
334 positive cells were rare at barriers, absent from parenchyma, and demyelination was not
335 observed in the brain (Fig. 4F) or spinal cord of immunized DR15 MS mice.
336
337 To determine whether CNS immune infiltration in the immunized mice was secondary to
338 levels of GVHD inflammation in the periphery, we performed semi-quantitative analysis of
339 liver and lung sections with H&E staining. Immunized DR13 MS mice showed the lowest levels
340 of immune cell infiltration in liver and lung, DR15 MS1 mice intermediate levels, and DR15 HI
341 highest levels (Supplementary Fig. 2). Results revealed an inverse relationship between
342 peripheral and CNS inflammation in the DR15 HI and MS mice, with DR15 HI mice showing
343 highest peripheral and relatively lower CNS involvement, while DR15 MS mice showed the
344 highest CNS and relatively lower peripheral inflammation. These results show that
345 immunization of DR15 HI and DR15 MS mice with myelin peptides equally induced spinal cord
346 white matter inflammatory lesions, and uniquely induced large confluent brain white and grey
347 matter lesions in DR15 MS mice. Taken together, our results show that PBMC from DR15-
348 positive MS patients show increased propensity to induce inflammatory CNS lesions
349 compared to PBMC from a DR13-positive MS patient or a DR15-positive healthy individual.
350
351 **Discussion**
352 Here we show that PBMC from RRMS and healthy donors with different HLA-DRB1 genotypes
353 have the potential to efficiently engraft B2m-NOG mice with human T and B lymphocytes and
354 to induce sub-clinical CNS inflammation dominated by $hCD8^+$ T cells in the brain and the spinal
355 cord. Specifically, mice engrafted with PBMC from DR15-positive MS and healthy donors, and
356 not from a DR13-positive MS donor, showed spontaneous brain and spinal cord infiltration by
357 $hCD8^+$ T cells, and increased infiltration by $hCD4^+$ following immunization for EAE. CNS
358 inflammation was more severe in mice engrafted with PBMC from several DR15-positive MS
359 donors. These mice uniquely developed large human T cell lesions in brain regions including
360 the corpus callosum with or without immunization with myelin peptides using an EAE
361 protocol. Human T cell lesions were associated with locally activated mouse microglia and
362 astrocytes, but notably lacked infiltrating human or mouse monocytes and demyelination,
363 and therefore did not lead to clinical symptoms of EAE or other neurological defects.
364
365 PBMC humanized B2m-NOG mice developed several hallmark features of MS that are not
366 readily reproduced in conventional animal models, such as EAE. First, brain immune infiltrates
367 in DR15 MS engrafted mice were enriched for $hCD8^+$ over $hCD4^+$ T cells, even though the B2m-
368 NOG model is characterized by increased engraftment of $CD4^+$ over $CD8^+$ T cells (18) (Figure
369 1B). The preferential infiltration of the CNS parenchyma by $CD8^+$ T cells and the presence of
370 inflammatory lesions in the brain white and grey matter in our model are both features of MS
371 (3,8,33). Second, T cell lesions and locally activated microglia and astrocytes, were observed
372 in brain white matter regions, particularly in the corpus callosum and optic tracts. Lesions in
373 the corpus callosum are important findings in MRI of MS patients and are correlated with
374 cognitive problems as well as disability in the upper limbs (34). Inflammation in the optic
375 tracts is often a first presenting symptom in MS and related disorders (35). Third, human
376 leukocytes were concentrated on the meninges and choroid plexus, notably in the

377 interventricular foramen connecting the lateral and third ventricles. The choroid plexus is an
378 important immunological site for immune surveillance and a site of $CD8^+$ T cell and
379 granulocyte involvement in progressive MS (36).
380
381 Nevertheless, MS is a complex disease and immunopathology was only partially reproduced
382 in the brain and the spinal cord of PBMC humanized B2m-NOG mice. Parenchymal lesions
383 contained both $hCD4^+$ and $hCD8^+$ T cells associated with locally activated microglia and
384 astrocytes, but there was poor engraftment by human monocytes in the blood, spleens or
385 CNS of both immunized and non-immunized B2m-NOG mice. Blood myeloid cells are short-
386 lived and constantly renewed by the bone marrow, so that human myeloid cells are nearly
387 absent in the commonly used PBMC-NSG model (18). In contrast, mouse $CD45^+$ cells
388 comprising very high proportions of $CD11b^+$ myeloid cells, $Ly6C^{hi}$ monocytes and $Ly6G^+$ cells,
389 were present in the blood of immunized and non-immunized NOD-*scid* mice, which are a
390 parental strain for B2m-NOG mice, and the non-immunized B2m-NOG mice prior to
391 engraftment. Nevertheless, mouse $CD45^+$ myeloid cells did not infiltrate the CNS of the
392 humanized mice, even after EAE induction. The absence of CNS-infiltrating human or mouse
393 monocytes in the PBMC humanized B2m-NOG mice NOG mice is most likely to be responsible
394 for the absence of clinical symptoms and demyelination in this system. Our results are
395 consistent with a previous study in which NSG mice were humanized with PBMC from healthy
396 donors and immunized for EAE (20). In that study, mice developed CNS inflammation with
397 infiltrating $CD4^+$ and $CD8^+$ T cells but did not show clinical symptoms or demyelination (20).
398 CNS-infiltrating $Ly6C^{hi}CCR2^+$ monocytes, which differentiate into inflammatory macrophages
399 locally in the CNS after being activated by T cells, are critical effector cells in EAE (22,37). These
400 cells are massively recruited into the periphery from the bone marrow following
401 immunization (23), and are likely to compete for space with engrafted human immune cells
402 before and after EAE induction. The use of immunodeficient NOG/NSG models expressing
403 human transgenes that would spport engraftment of human monocytes, or facilitate
404 communication of human T cells with mouse inflammatory monocytes (38,39), should allow
405 a more comprehensive modeling of MS immunopathology in humanized mice.
406
407 Another limitation for MS modeling in the B2m-NOG mice used in this study is the poor LN
408 structure and functioning that results from depletion of the common cytokine receptor γ-
409 chain gene (26). This deficiency was confirmed in this study by the absence of organized LN
410 and germinal follicles, and of anti-MOG IgG antibodies in the PBMC humanized B2m-NOG
411 mice immunized for EAE. Again, further development of available immunodeficient mouse
412 strains to promote LN organogenesis will be an important step for modeling MS
413 immunopathology in mice. In a previous study, NSG mice injected directly in the CNS with CSF
414 cells from MS patients (40) developed clinical symptoms, immune infiltration of the CNS and
415 demyelination, although differences in the route of administration of the transplanted cells
416 might explain the differences between our study and that of others (20).

417 Our observation that mice engrafted with PBMC from DR15-positive active RRMS patients
418 showed both spontaneous and EAE-inducible T cell lesions in the brainstem and spinal cord is
419 highly relevant in the context of previous data concerning this haplotype. HLA-DR2 has long
420 been associated with MS (41), with the DR15 haplotype being linked to earlier disease onset
421 (1,42). MHCII molecules present antigens to $CD4^+$ T cells, and DR15 is strongly associated with
422 the autoproliferation of peripheral $CD4^+$ T cells in MS patients (43). T cell autoproliferation is

423 mediated by memory B cells in a HLA-DR-dependent manner, and autoproliferating T cells are
424 increased in MS patients treated with natalizumab and enriched for brain-homing T cells (24).
425 In a recent study with humanized NSG mice, $CD34^+$ hematopoietic progenitor cells (HSC) from
426 DR15-positive donors induced higher peripheral T cell responses and alloreactivity compared
427 to HSC from DR15-negative donors, and increased $CD8^+$ T cell responses after EBV infection
428 (44). In our study human T cells isolated from DR13 MS mice showed positive T cell
429 proliferation responses to myelin peptides and hCD3 antibody. This provides proof-of-
430 principle for successful engraftment of functional human T cells in humanized mice. However,
431 none of the T cells isolated from DR15 MS1-5 mice showed further proliferation ex vivo, either
432 to myelin peptides or to polyclonal stimuli hCD3 antibody and PHA, possibly due to inherent
433 high levels of autoproliferation in these cells (24). Alternatively, CD4+ T cells may become
434 nonresponsive to anti-CD3 antibody once engrafted into B2m-NOG mice, as previously
435 reported in NOD-scid mice (25). Noteworthy is that MS patients suspected of recent or
436 ongoing reactivation of EBV (DR13 MS, DR15 MS3 and DR15 MS5; Table 1), showed the best
437 engraftment of $hCD19^+$ B lymphocytes in mice, and that both DR15 MS3 and DR15 MS5 mice
438 showed multiple CNS lesions.

439 There is now strong evidence that EBV infection plays a major role in MS pathogenesis (45),
440 acting synergistically with DR15 to increase the likelihood of developing MS (41). DR15
441 individuals with specific antibody reactivity to EBNA1 (amino acid 385–420) have 24-fold
442 increased risk for MS (46). Anti-EBNA-1 antibodies present high homology and react with
443 several CNS antigens, such as αB-crystallin, MBP, anoctamin 2 and more recently glial cell
444 adhesion molecule (47–50). Nevertheless, positive correlations between the DR15 haplotype,
445 T cell autoproliferation, EBV and the development of brain lesions in humanized mice remain
446 to be formally tested in a larger study using greater numbers of DR15-positive MS donors
447 compared to DR15 negative MS and DR15-positive healthy controls, together with the
448 measurement of basal levels of T cell proliferation in the peripheral blood of the PBMC
449 donors.
450
451 In summary, PBMC humanized B2m-NOG mice show partial representation of MS
452 immunopathology that is not reproduced in conventional animal models such as EAE,
453 particularly the development of $hCD8^+$ lesions in the grey and white matter of the brain and
454 spinal cord. New immunodeficient mouse strains developed to promote human monocyte
455 engraftment and the development of organized LN therefore hold great promise for
456 comprehensive modelling of MS immunopathology. An important outcome of this study is
457 that PBMC humanized B2m-NOG mice highlight the variability between the different human
458 PBMC donors, and therefore represent a simple and rapid approach for generating
459 personalized immune models for drug screening.
460
461
462 **Materials & Methods**
463 **MS patients and healthy subjects**
464 Blood donors were selected from a Hellenic MS patient cohort attending the MS outpatient
465 clinic at Aeginition University Hospital of the National and Kapodistrian University of Athens
466 (NKUA) School of Medicine, supervised by Dr. Maria Anagnostouli and genotyped for the HLA-
467 DRB1 allele, at the Research Immunogenetics Laboratory, of the same Hospital, as previously
468 described (21) (Table 1). Six patients with long-term RRMS recently presenting with highly

469 active disease since the last dose of immunomodulatory therapy (natalizumab) were selected.
470 Natalizumab treatment was chosen as a criteria for this study because it blocks lymphocyte
471 migration to the brain, thereby increasing circulating T and B lymphocytes (51). One patient
472 was DR13-positive (DR13 MS), and five were DR15-positive (DR15 MS). The DR13-positive
473 patient additionally received cortisone treatment 1 month prior to sampling because of high
474 disease activity. A healthy DR15-matched healthy individual (DR15 HI) was selected as control.
475 Donor characteristics, including viral infections and EBV status are listed in Table 1. Blood
476 samples were obtained from MS patients and healthy individuals under signed informed
477 consent in accordance with the Declaration of Helsinki and approval from the Institutional
478 Ethics Committee of Aeginition Hospital, NKUA (Protocol No: 7BSH46Y8N2-B66, 13/05/2015).

479 **PBMC isolation**

480 Fresh peripheral blood (50 ml) was collected in EDTA-treated polypropylene tubes and PBMC
481 were isolated under Ficoll-Histopaque®-1077 gradient centrifugation (Sigma-Aldrich). Buffy
482 coats containing blood leukocytes were washed with 2% FBS in PBS. Erythrocytes were
483 removed using Quicklysis™ erythrocyte lysis buffer (Cytognos) and leukocytes were washed
484 with 2% FBS in PBS. Before transfer of PBMC into mice, we compared several protocols for
485 preparation of human PBMC using blood from a healthy individual, specifically, 1) PBMC
486 isolated from fresh blood on the day of transfer, 2) PBMC isolated from blood after 3 days'
487 storage at 4°C, 3) PBMC cultured for 24 h in complete RPMI-1640 after snap freezing of fresh
488 PBMC and thawing. Cell viability and analysis of immune cell populations by flow cytometry
489 showed that freshly isolated PBMC gave the best results and were used for transfer in this
490 study (Supplementary Table 2).
491
492 **EBV antibody responses in human blood**

493 Blood plasma from the DR13 MS, DR15 MS and DR15 HI donors was analyzed for EBV antibody
494 responses using the following ELISA tests: ELISA-VIDITESTS anti-VCA EBV IgG (ODZ-265), anti-
495 VCA IgM (ODZ-005), and anti-VCA IgA (ODZ-096), anti-EA (D) EBV IgG (ODZ-006), anti-EBNA-1
496 EBV IgM (ODZ-002) and anti-EBNA-1 EBV IgG (ODZ-001) (Vidia). Standardized criteria for the
497 clinical interpretation of EBV antibody responses are shown in Supplementary Table 1C.
498
499 **Mice**

500 Ten-to-twelve-week-old female immunodeficient B2m-NOD/Shi - *scid IL2rg^{null}* (B2m-NOG)
501 mice (stock number 14957-F: NOD.Cg-B2m<em1Tac> Prkdc<scid>Il2rg<tm1Sug>JicTac;
502 Taconic Biosciences) were used for transfer of freshly isolated human PBMC. These mice lack
503 mature T, B, and NK cells and lack MHC class I molecules. Previous studies show that an
504 equivalent mouse strain, *NOD.Cg-Prkdc^{scid}Il2rg^{tm1Wjl}B2m^{tm1Unc}/Sz* (NSG β2m^{null}; The Jackson
505 laboratory) facilitates the engraftment of CD4^{+} over CD8^{+} T cells and exhibits delayed onset
506 of graft versus host disease (17,18). NOD.CB17-Prkdc scid/NCrHsd (Envigo) were used for
507 investigation of peripheral mouse myeloid cell populations in a related severely
508 immunodeficient mouse strain by flow cytometry.

509 Mice were transplanted via tail vein injection with 10x10^{6} PBMC in 200 μL PBS on the same
510 day as cell isolation from fresh peripheral human blood. Mice were assessed daily for
511 symptoms of GVHD, such as fur ruffling, hunched posture, reduced mobility and tachypnea
512 (28), as well as for any spontaneous neurological deficits (27).

513 All experiments were performed under sterile conditions in the Department of Animal Models
514 for Biomedical Research of the Hellenic Pasteur Institute. Mice were housed in a specific
515 pathogen-free facility in microisolator cages and given *ad libitum* UV-sterilized standard
516 chow, acidified water and gels for hydration. The experiments complied with ARRIVE
517 guidelines and were in accordance with the local Ethical Committee guidelines on the use of
518 experimental animals at the Hellenic Pasteur Institute, were approved by the national
519 authorities and complied to EU Directive 2010/63/EU for animal experiments.

520 **Immunization with myelin peptides**
521 Peptides MBP83-99, MOG1-20, and mMOG35-55 and hMOG35-55 (S42 in mMOG, P42 in
522 hMOG), were synthesized as previously described (52). In a previous study, we found that
523 humanized HLA-DR2b transgenic mice lacking all mouse MHCII genes required greater
524 amounts of peptide antigen to induce clinical EAE than wild-type B6 mice (21). Due to limited
525 numbers of B2m-NOG mice available for this study, several EAE protocols were first tested
526 using wild-type B6 mice, mainly to exclude the possibility of toxicity at high peptide doses.
527 Briefly, 8-week-old female B6 mice were immunized by subcutaneous (s.c.) tail-base injection
528 of 37 µg (our standard EAE protocol) or 200 µg mMOG35-55, or a myelin peptide antigen
529 cocktail containing 200 µg each of mMOG35-55, hMOG35-55, MOG1-20 and MBP83-99,
530 dissolved in 100 µl saline and emulsified in an equal volume of Freund's complete adjuvant
531 (FCA) (Sigma-Aldrich). FCA was supplemented with 400 µg/injection of H37Ra *Mycobacterium*
532 *tuberculosis* (Difco, BD Biosciences). All mice, except those immunized using the standard
533 protocol, received an identical boost immunization 7 days later. The immunized mice also
534 received intraperitoneal (i.p.) injections of 200 ng of *Bordetella pertussis* toxin (PTx) (Sigma-
535 Aldrich) at the time of each immunization and 48 h later. All mice developed clinical symptoms
536 of EAE with no evidence of increased morbidity or mortality at high peptide doses. For this
537 reason, the high-dose peptide cocktail was chosen for immunization of groups of 12-14-week-
538 old PBMC humanized B2m-NOG mice on dpt 14 in EAE experiment 1. In EAE experiment 2,
539 groups of 12-14-week-old PBMC humanized B2m-NOG were immunized once, using 100 µg
540 each peptide/mouse, to reduce the possibility of immune tolerance. Mice were monitored
541 daily for the clinical symptoms of EAE according to criteria commonly used for scoring EAE: 0,
542 normal; 1, limp tail; 2, hind limb weakness; 3, hind limb paralysis; 4, forelimb paralysis; 5,
543 moribund or dead (0.5 gradations represent intermediate scores) (21). Mice were also
544 monitored for signs of other neurological deficits (27).
545
546 **MOG antibody responses in PBMC humanized mouse blood**
547 Peripheral blood was collected from immunized and non-immunized mice at sacrifice on dpt
548 42, and sera collected for analysis of antibody responses. Samples were screened for IgG
549 antibodies against MOG, using indirect immunofluorescence assays (IFA). Sera were analyzed
550 at a starting dilution of 1:10, on EU 90 cells transfected with MOG protein and on EU 90
551 control transfected cells, according to the manufacturer instructions (Euroimmun, Lubeck,
552 Germany). Visualization and evaluation of IFA results were performed under a fluorescence
553 microscope (Zeiss, Axioskop 40).
554
555 **Flow cytometry**
556 Fresh peripheral blood samples from the MS and HI donors were analyzed by FACS using a
557 panel of immune cell marker antibodies. To monitor immune cell populations, 3 ml fresh
558 peripheral blood was collected in EDTA tubes and a 100 µl aliquot was used for flow

559 cytometry. Erythrocyte lysis was achieved with with Quicklysis™ (Cytognos) for 25 min. Cells
560 were washed and incubated with an antibody mixture for human immune cell markers BV-
561 510-hCD45 (clone 2D1), APC-Cyanine 7-hCD3 (clone HIT3a), PE-Cyanine 7-hCD4 (clone
562 A161A1), PerCP-hCD8 (clone SK1), PE-hCD19 (clone 4G7), FITC-hCD56 (clone 5.1H11), APC-
563 hCD66b (clone G1OF5), BV-421-hCD14 (clone HCD14) (all from Biolegend), for 30 min at 4 °C
564 (Supplementary Table 1A). To monitor engraftment of human immune cells in B2m-NOG
565 mice, peripheral blood was collected in heparin tubes from the tail vein at dpt 7, 13 and 42.
566 Erythrocyte lysis and incubation with antibody mixture was performed as for fresh human
567 blood above, except that the APC-hCD66b antibody was replaced by mouse APC-CD45 (clone
568 30-F11) (Biolegend) (Supplementary Table 1A). Data was acquired with FACSCelesta™,
569 FACSCanto™ II or FACSMelody™ cytometer and analyzed with FACSDiva™ (BD) and FlowJo
570 software (Tree Star, Inc.).
571
572 For intracellular staining of IFN-γ, splenocytes were isolated at sacrifice at dpt 42 as described
573 above, and cells were stimulated with phorbol 12-myristate 13 acetate (PMA) (20 ng/ml,
574 Sigma-Aldrich) and ionomycin (1µg/ml, Sigma-Aldrich) and treated with brefeldin-A (5µg/ml,
575 Sigma-Aldrich) for 3 h at 37°C/5% CO2 in order to disrupt Golgi-mediated transport. Cells were
576 fixed with 2% PFA in FBS, permeabilized using 0.5% wt/vol saponin, and stained with PerCP-
577 Cyanine 5.5-CD3 (clone HIT3a, Biolegend), antibodies for APC-CD4 (clone RPA-T4, BD
578 Biosciences), PerCP-CD8 (clone SK1, Biolegend), and PE-IFN-γ (clone B27; BD Biosciences) and
579 PE-IL-17A (clone eBio64DEC17, eBioscience). Data acquisition was performed using a
580 FACSCalibur™ cytometer and analyzed with FlowJo software (Tree Star, Inc.).
581
582 **T cell proliferation assay**
583 Spleens were isolated at sacrifice and cells mechanically separated in RPMI (Invitrogen Life
584 Technologies) containing 10% heat-inactivated FCS. To obtain single cell suspensions, the
585 washed homogenate was passed through a 70 µm cell strainer and erythrocyte lysis was
586 performed with Gey's erythrocyte lysis buffer for 5 min. The reaction was stopped with RPMI
587 1640/FCS. Washed splenocytes at a concentration of 10^7 cells/mL in PBS were incubated with
588 5 µM carboxylfluorescein succimidyl ester (CFSE, V12883, Thermofisher) for 15 min at 37°C.
589 Cells were washed and PBS/2% FCS was applied for 30 min at 37°C to stop the reaction. Cells
590 were washed and resuspended in RPMI 1640/FCS with 50 µM 2-mercaptoethanol (Sigma-
591 Aldrich) at concentration of 10^6 cells/ml. The cells were stimulated with in triplicates in round-
592 bottom 96-well plates with a myelin peptide antigen cocktail containing 30 µg/ml each
593 mMOG35-55, hMOG35-55, MOG1-20 and MBP83-99 for 120 h. Negative control cells were
594 incubated with medium only, and positive control cells were incubated in plates coated with
595 anti-CD3 (1µg/ml) (clone HIT3a, BD Biosciences) or PHA (2 µg/ml) (Sigma-Aldrich). Results
596 were expressed as cell division index which is the ratio of %$CFSE^{low}$ splenocytes (proliferating
597 splenocytes) cultured with peptides or anti-CD3 to the of %$CFSE^{low}$ splenocytes cultured with
598 medium only. Data acquisition was performed using a FACSCalibur™ cytometer and analyzed
599 with FlowJo software (Tree Star, Inc.)
600
601 **Histopathology and Immunohistochemistry**
602 Mice were transcardially perfused with ice-cold PBS at sacrifice on dpt 42 by carbon dioxide
603 inhalation. Brains, spinal cords and peripheral tissues (including lung, liver and inguinal fat
604 tissue) were dissected and post-fixed in 4% paraformaldehyde fixative (PFA) overnight at 4°C.
605 Tissues were embedded in paraffin and 5µm sections and used for immunohistochemistry

606 and histopathology. Inflammation in peripheral tissues was visualized by haematoxylin and
607 eosin (H&E) using standard techniques. Immune cell infiltration and inflammation of brain
608 and spinal cord was visualized by immunohistochemistry using antibodies specific for hCD45,
609 hCD4, hCD8, mCD45, and mouse Iba1 and GFAP followed by biotinylated secondary Abs,
610 horseradish peroxidase-labeled avidin-biotin complex, and signal development using 3'3'-
611 diaminobenzidine. Nuclei were counterstained with hematoxylin. Images were captured with
612 an Olympus DP71 microscope digital camera using cell^A imaging software (Soft Imaging
613 System GmbH). High resolution immunofluorescence imaging was performed by confocal
614 microscopy using paraffin sections immunostained with marker antibodies for myelin (MBP),
615 microglia (Iba1) followed by anti-rat CF-647- (Biotrium) and anti-rabbit AlexaFluor 568-
616 (Invitrogen) labelled secondary antibodies, respectively. Nuclei were counterstained with
617 DAPI. A Leica TCS SP8 confocal microscope was used to acquire fluorescent images.
618
619 **Statistical Analysis**
620 Data were processed using Microsoft Excel, and statistical analysis was performed with
621 Graphpad Prism 8. Figures were made using Adobe Illustrator V24.3 Data was analyzed with
622 Student's t test and results are presented as means ± SEM. Results were considered
623 statistically significant when $p \leq 0.05$. Graphical abstract was created using BioRender.com

624 **Data availability statement**
625 The raw data supporting the conclusions of this manuscript will be made available by the
626 authors, without undue reservation, to any qualified researcher.
627
628 **Conflict of interest statement**
629 The authors report no conflict of interest.
630
631 **Ethics approvals**
632 The studies involving human participants were reviewed and approved by the Scientific
633 Committee of Aeginition Hospital, National and Kapodistrian University of Athens, Greece.
634 Licence 283/13-05-2015ADA: 7BΣH46Y8N2-B66. The patients/participants provided their
635 written informed consent to participate in this study. The animal study was reviewed and
636 approved by Committee for Evaluation of Experimental Procedures, Department of
637 Experimental Animal Models, Hellenic Pasteur Institute (Presided by Dr P Andriopoulos
638 pandriopoulos@patt.gov.grfor the Hellenic Republic, General Secretariat for Agricultural
639 Economy, Veterinary and Licenses). Licence numbers 770851/27-11-2019 and 1343917/02-
640 11-2023.
641
642 **Patient consent statement**
643 Written informed consent was obtained from the human individual(s) for the publication of
644 any potentially identifiable images or data included in this article.
645
646 **Authors contributions**
647 IP designed, set-up and performed experimental protocols for PBMC preparation and
648 humanization of B2m-NOG mice, monitored mice for clinical symptoms and performed
649 immunohistochemical analysis of CNS tissues, analysed results and prepared figures; MK
650 performed quantitative immunohistochemical analysis of CNS tissues, analysed results,
651 monitored EAE mice for clinical symptoms and prepared figures; AD designed and performed

EAE experiments, monitored mice for clinical symptoms, performed immunohistochemistry of LN tissues and FACS analyses of humanized mice, analysed results and prepared figures; VG performed FACS analysis and EBV ELISA on fresh human donor blood samples; LD designed human FACS antibody panel, performed analyses of human and mouse blood and analysed results; NM collected and co-ordinated delivery of human donor blood samples; FB performed histological analysis of peripheral humanized mouse tissues and evaluated GVHD; TT designed, synthesized, purified and characterized myelin peptide analogues; MA performed HLA genotyping, selected patients for this study, and supervised Hellenic MS patient cohort; LP was responsible for overall experimental design and management of project, analysed and interpreted data, wrote paper. All authors contributed to the article, edited, and approved the submitted version.

Funding

This research was co-financed by European Union and Greek national funds by The Management and Implementation Authority for Research, Technological Development and Innovation Actions (MIA-RTDI/ EYDE-ETAK) of the Hellenic Ministry of Development and Investments, through the Operational Program Competitiveness, Entrepreneurship and Innovation, under the call RESEARCH – CREATE – INNOVATE (project code T1EDK-01859; acronym AKESO) to LP. Research was also supported by the Hellenic General Secretariat for Research and Innovation (G.S.R.I.) Flagship Action for Neurodegenerative Diseases on the basis of Personalized Medicine (Project code 2018ΣΕ01300001, acronym EDIA-N) to LP. B2m-NOG mouse availability was supported by Vianex, SA, Athens, Greece. VG was supported by the Hellenic Pasteur Institute through a "NOSTOS FOUNDATION TRUST FUND" PhD fellowship.

Acknowledgements

We wish to thank Ivan Gladwyn-Ng and Dimitri Gimnopoulos (Taconic Biosciences) for providing B2m-NOG mice and expert scientific support, Konstantinos Kambas (Molecular Genetics Lab, HPI), Maritsa Margaroni (Flow Cytometry Unit, HPI), Katerina Nanou and George Kollias (BSRC Alexander Fleming) for support with the flow cytometry analyses, Maria Belimezi and Manolis Angelakis (Diagnosis Dept, HPI) for screening mouse plasma for anti-hMOG IgG antibodies, and Maria Avloniti for contributing research material. We especially thank Eirini Fragkiadaki and Ariadne Karles, and other members of the Department of Experimental Animals for Biomedical Research of HPI for their help and expert support in maintenance of the B2m-NOG mice, and the training of experimenters in mouse familiarization techniques during these experiments.

690 **References**

691 1. International Multiple Sclerosis Genetics C, Wellcome Trust Case Control C, Sawcer S,
692 Hellenthal G, Pirinen M, Spencer CC, et al. Genetic risk and a primary role for cell-
693 mediated immune mechanisms in multiple sclerosis. Nature [Internet].
694 2011;476(7359):214–9. Available from:
695 http://www.ncbi.nlm.nih.gov/pubmed/21833088
696 2. Beecham AH, Patsopoulos NA, Xifara DK, Davis MF, Kemppinen A, Cotsapas C, et al.
697 Analysis of immune-related loci identifies 48 new susceptibility variants for multiple
698 sclerosis. 2013;45(11):1353–60.
699 3. Lassmann H. The changing concepts in the neuropathology of acquired demyelinating
700 central nervous system disorders. Curr Opin Neurol. 2019/03/21. 2019;32(3):313–9.
701 4. Regen T, Waisman A. Modeling a complex disease: Multiple sclerosis-Update 2020.
702 Adv Immunol. 2021;149:25–34.
703 5. Schreiner B, Heppner FL, Becher B. Modeling multiple sclerosis in laboratory animals.
704 Semin Immunopathol. 2009 Nov;31(4):479–95.
705 6. Attfield KE, Dendrou CA, Fugger L. Bridging the gap from genetic association to
706 functional understanding: the next generation of mouse models of multiple sclerosis.
707 Immunol Rev. 2012 Jul;248(1):10–22.
708 7. Lassmann H, Bradl M. Multiple sclerosis: experimental models and reality. Acta
709 Neuropathol. 2016/10/22. 2017;133(2):223–44.
710 8. Babbe H, Roers A, Waisman A, Lassmann H, Goebels N, Hohlfeld R, et al. Clonal
711 expansions of CD8(+) T cells dominate the T cell infiltrate in active multiple sclerosis
712 lesions as shown by micromanipulation and single cell polymerase chain reaction. J
713 Exp Med. 2000 Aug;192(3):393–404.
714 9. Wiendl H, Hohlfeld R. Multiple sclerosis therapeutics: unexpected outcomes clouding
715 undisputed successes. Neurology [Internet]. 2009;72(11):1008–15. Available from:
716 http://www.ncbi.nlm.nih.gov/pubmed/19289741
717 10. Wekerle H, Flügel A, Fugger L, Schett G, Serreze D. Autoimmunity's next top models.
718 Nat Med. 2012;18(1):66–70.
719 11. Mestas J, Hughes CCW. Of mice and not men: differences between mouse and human
720 immunology. J Immunol. 2004 Mar;172(5):2731–8.
721 12. Hauser SL, Bar-Or A, Comi G, Giovannoni G, Hartung H-P, Hemmer B, et al.
722 Ocrelizumab versus Interferon Beta-1a in Relapsing Multiple Sclerosis. N Engl J Med.
723 2017 Jan;376(3):221–34.
724 13. Li R, Bar-Or A. The Multiple Roles of B Cells in Multiple Sclerosis and Their
725 Implications in Multiple Sclerosis Therapies. Cold Spring Harb Perspect Med. 2019
726 Apr;9(4).
727 14. Allen TM, Brehm MA, Bridges S, Ferguson S, Kumar P, Mirochnitchenko O, et al.
728 Humanized immune system mouse models: progress, challenges and opportunities.
729 Vol. 20, Nature immunology. United States; 2019. p. 770–4.
730 15. Nagatani M, Kodera T, Suzuki D, Igura S, Fukunaga Y, Kanemitsu H, et al. Comparison
731 of biological features between severely immuno-deficient NOD/Shi-scid Il2rg(null)
732 and NOD/LtSz-scid Il2rg(null) mice. Exp Anim. 2019 Nov;68(4):471–82.
733 16. Willinger T, Rongvaux A, Takizawa H, Yancopoulos GD, Valenzuela DM, Murphy AJ, et
734 al. Human IL-3/GM-CSF knock-in mice support human alveolar macrophage
735 development and human immune responses in the lung. Proc Natl Acad Sci U S A.
736 2011 Feb;108(6):2390–5.

17. Morillon YM 2nd, Sabzevari A, Schlom J, Greiner JW. The Development of Next-generation PBMC Humanized Mice for Preclinical Investigation of Cancer Immunotherapeutic Agents. Anticancer Res. 2020 Oct;40(10):5329–41.
18. King MA, Covassin L, Brehm MA, Racki W, Pearson T, Leif J, et al. Human peripheral blood leucocyte non-obese diabetic-severe combined immunodeficiency interleukin-2 receptor gamma chain gene mouse model of xenogeneic graft-versus-host-like disease and the role of host major histocompatibility complex. Clin Exp Immunol. 2009 Jul;157(1):104–18.
19. Morillon YMI, Smalley Rumfield C, Pellom ST, Sabzevari A, Roller NT, Horn LA, et al. The Use of a Humanized NSG-β2m(-/-) Model for Investigation of Immune and Anti-tumor Effects Mediated by the Bifunctional Immunotherapeutic Bintrafusp Alfa. Front Oncol. 2020;10:549.
20. Zayoud M, El Malki K, Frauenknecht K, Trinschek B, Kloos L, Karram K, et al. Subclinical CNS inflammation as response to a myelin antigen in humanized mice. J neuroimmune Pharmacol Off J Soc NeuroImmune Pharmacol. 2013 Sep;8(4):1037–47.
21. Dagkonaki A, Avloniti M, Evangelidou M, Papazian I, Kanistras I, Tseveleki V, et al. Mannan-MOG35-55 Reverses Experimental Autoimmune Encephalomyelitis, Inducing a Peripheral Type 2 Myeloid Response, Reducing CNS Inflammation, and Preserving Axons in Spinal Cord Lesions. Front Immunol. 2020;11:575451.
22. King IL, Dickendesher TL, Segal BM. Circulating Ly-6C+ myeloid precursors migrate to the CNS and play a pathogenic role during autoimmune demyelinating disease. Blood. 2009 Apr;113(14):3190–7.
23. Dagkonaki A, Papalambrou A, Avloniti M, Gkika A, Evangelidou M, Androutsou M-E, et al. Maturation of circulating Ly6C(hi)CCR2(+) monocytes by mannan-MOG induces antigen-specific tolerance and reverses autoimmune encephalomyelitis. Front Immunol. 2022;13:972003.
24. Jelcic I, Al Nimer F, Wang J, Lentsch V, Planas R, Jelcic I, et al. Memory B Cells Activate Brain-Homing, Autoreactive CD4(+) T Cells in Multiple Sclerosis. Cell. 2018/09/04. 2018;175(1):85-100.e23.
25. Wagar EJ, Cromwell MA, Shultz LD, Woda BA, Sullivan JL, Hesselton RM, et al. Regulation of human cell engraftment and development of EBV-related lymphoproliferative disorders in Hu-PBL-scid mice. J Immunol. 2000 Jul;165(1):518–27.
26. Mebius RE. Organogenesis of lymphoid tissues. Nat Rev Immunol. 2003 Apr;3(4):292–303.
27. Guyenet SJ, Furrer SA, Damian VM, Baughan TD, La Spada AR, Garden GA. A simple composite phenotype scoring system for evaluating mouse models of cerebellar ataxia. J Vis Exp. 2010 May;(39).
28. Cooke KR, Kobzik L, Martin TR, Brewer J, Delmonte JJ, Crawford JM, et al. An experimental model of idiopathic pneumonia syndrome after bone marrow transplantation: I. The roles of minor H antigens and endotoxin. Blood. 1996 Oct;88(8):3230–9.
29. Pette M, Fujita K, Kitze B, Whitaker JN, Albert E, Kappos L, et al. Myelin basic protein-specific T lymphocyte lines from MS patients and healthy individuals. Neurology. 1990/11/01. 1990;40(11):1770–6.
30. Ota K, Matsui M, Milford EL, Mackin GA, Weiner HL, Hafler DA. T-cell recognition of

784 an immunodominant myelin basic protein epitope in multiple sclerosis. Nature.
785 1990/07/12. 1990;346(6280):183–7.
786 31. Kerlero de Rosbo N, Milo R, Lees MB, Burger D, Bernard CC, Ben-Nun A. Reactivity to
787 myelin antigens in multiple sclerosis. Peripheral blood lymphocytes respond
788 predominantly to myelin oligodendrocyte glycoprotein. J Clin Invest. 1993/12/01.
789 1993;92(6):2602–8.
790 32. Cao Y, Goods BA, Raddassi K, Nepom GT, Kwok WW, Love JC, et al. Functional
791 inflammatory profiles distinguish myelin-reactive T cells from patients with multiple
792 sclerosis. Sci Transl Med [Internet]. 2015;7(287):287ra74. Available from:
793 http://www.ncbi.nlm.nih.gov/pubmed/25972006
794 33. Wagner CA, Roqué PJ, Mileur TR, Liggitt D, Goverman JM. Myelin-specific CD8+ T cells
795 exacerbate brain inflammation in CNS autoimmunity. J Clin Invest. 2020
796 Jan;130(1):203–13.
797 34. Ozturk A, Smith SA, Gordon-Lipkin EM, Harrison DM, Shiee N, Pham DL, et al. MRI of
798 the corpus callosum in multiple sclerosis: association with disability. Mult Scler. 2010
799 Feb;16(2):166–77.
800 35. Jakimovski D, Bittner S, Zivadinov R, Morrow SA, Benedict RH, Zipp F, et al. Multiple
801 sclerosis. Lancet (London, England). 2024 Jan;403(10422):183–202.
802 36. Rodríguez-Lorenzo S, Konings J, van der Pol S, Kamermans A, Amor S, van Horssen J,
803 et al. Inflammation of the choroid plexus in progressive multiple sclerosis:
804 accumulation of granulocytes and T cells. Acta Neuropathol Commun. 2020
805 Feb;8(1):9.
806 37. Ajami B, Bennett JL, Krieger C, McNagny KM, Rossi FM V. Infiltrating monocytes
807 trigger EAE progression, but do not contribute to the resident microglia pool. Nat
808 Neurosci. 2011 Jul;14(9):1142–9.
809 38. Codarri L, Greter M, Becher B. Communication between pathogenic T cells and
810 myeloid cells in neuroinflammatory disease. Trends Immunol. 2013 Mar;34(3):114–9.
811 39. El-Behi M, Ciric B, Dai H, Yan Y, Cullimore M, Safavi F, et al. The encephalitogenicity of
812 T(H)17 cells is dependent on IL-1- and IL-23-induced production of the cytokine GM-
813 CSF. Nat Immunol. 2011 Jun;12(6):568–75.
814 40. Saeki Y, Mima T, Sakoda S, Fujimura H, Arita N, Nomura T, et al. Transfer of multiple
815 sclerosis into severe combined immunodeficiency mice by mononuclear cells from
816 cerebrospinal fluid of the patients. Proc Natl Acad Sci U S A. 1992 Jul;89(13):6157–61.
817 41. Nielsen TR, Rostgaard K, Askling J, Steffensen R, Oturai A, Jersild C, et al. Effects of
818 infectious mononucleosis and HLA-DRB1*15 in multiple sclerosis. Mult Scler. 2009
819 Apr;15(4):431–6.
820 42. Masterman T, Ligers A, Olsson T, Andersson M, Olerup O, Hillert J. HLA-DR15 is
821 associated with lower age at onset in multiple sclerosis. Ann Neurol. 2000
822 Aug;48(2):211–9.
823 43. Mohme M, Hotz C, Stevanovic S, Binder T, Lee J-H, Okoniewski M, et al. HLA-DR15-
824 derived self-peptides are involved in increased autologous T cell proliferation in
825 multiple sclerosis. Brain. 2013 Jun;136(Pt 6):1783–98.
826 44. Zdimerova H, Murer A, Engelmann C, Raykova A, Deng Y, Gujer C, et al. Attenuated
827 immune control of Epstein-Barr virus in humanized mice is associated with the
828 multiple sclerosis risk factor HLA-DR15. Eur J Immunol. 2021 Jan;51(1):64–75.
829 45. Bjornevik K, Cortese M, Healy BC, Kuhle J, Mina MJ, Leng Y, et al. Longitudinal analysis
830 reveals high prevalence of Epstein-Barr virus associated with multiple sclerosis.

831 Science. 2022 Jan;375(6578):296–301.
832 46. Sundström P, Nyström M, Ruuth K, Lundgren E. Antibodies to specific EBNA-1
833 domains and HLA DRB1*1501 interact as risk factors for multiple sclerosis. J
834 Neuroimmunol. 2009 Oct;215(1–2):102–7.
835 47. Lanz T V, Brewer RC, Ho PP, Moon J-S, Jude KM, Fernandez D, et al. Clonally expanded
836 B cells in multiple sclerosis bind EBV EBNA1 and GlialCAM. Nature. 2022
837 Mar;603(7900):321–7.
838 48. Tengvall K, Huang J, Hellström C, Kammer P, Biström M, Ayoglu B, et al. Molecular
839 mimicry between Anoctamin 2 and Epstein-Barr virus nuclear antigen 1 associates
840 with multiple sclerosis risk. Proc Natl Acad Sci U S A. 2019 Aug;116(34):16955–60.
841 49. Hecker M, Fitzner B, Wendt M, Lorenz P, Flechtner K, Steinbeck F, et al. High-Density
842 Peptide Microarray Analysis of IgG Autoantibody Reactivities in Serum and
843 Cerebrospinal Fluid of Multiple Sclerosis Patients. Mol Cell Proteomics. 2016
844 Apr;15(4):1360–80.
845 50. Jog NR, McClain MT, Heinlen LD, Gross T, Towner R, Guthridge JM, et al. Epstein Barr
846 virus nuclear antigen 1 (EBNA-1) peptides recognized by adult multiple sclerosis
847 patient sera induce neurologic symptoms in a murine model. J Autoimmun. 2020
848 Jan;106:102332.
849 51. Yednock TA, Cannon C, Fritz LC, Sanchez-Madrid F, Steinman L, Karin N. Prevention of
850 experimental autoimmune encephalomyelitis by antibodies against alpha 4 beta 1
851 integrin. Nature. 1992 Mar;356(6364):63–6.
852 52. Tapeinou A, Androutsou ME, Kyrtata K, Vlamis-Gardikas A, Apostolopoulos V,
853 Matsoukas J, et al. Conjugation of a peptide to mannan and its confirmation by tricine
854 sodium dodecyl sulfate-polyacrylamide gel electrophoresis. Anal Biochem.
855 2015/06/17. 2015;485:43–5.
856
857
858

859 **Table 1**

860

HLA genotype Diagnosis (donor type)	**G**	**Age**	**MS duration (y)**	**Therapies**	**Relapse (12/24 m)**	**MRI Brain/Gd**	**MRI Spine/Gd**	**EDSS**	**Viral infections (titre)**	**EBV clinical interpretation** (Suppl. Table 1C)	**T cell responses** (21)
DR13 1302/1303 RRMS (donor for DR13 MS mice)	F	42	27	Azathioprine Interferon beta-1a Interferon beta-1b Fingolimod Natalizumab (5 months) Cortisone (for 1 month prior to sampling)	1/1 Last relapse 05/23	(+) stable	(+) GD (+)	2.5	**JC**$^{+}$ (1.24) **EBV** VCA IgG^{+} **EBV** VCA IgM^{-} **EBV** VCA IgA^{+} **EBV** EA IgG^{+} **EBV** EBNA1 IgG^{+} **EBV** EBNA1 IgM^{-}	Suspect recent or ongoing reactivation	MBP83-99 hMOG35-55 [Patient 17(21)]
DR15 0402/1501 RRMS (donor for DR15 MS1 mice)	F	38	15	Interferon beta-1a Fingolimod Natalizumab (24 months) To Cladribine (after sampling)	1/1 No relapse during the last year	(+) stable	(+) stable	2.5	**JC**$^{+}$ (1.47) **EBV** VCA IgG^{+} **EBV** VCA IgM^{-} **EBV** VCA IgA^{-} **EBV** EA IgG^{-} **EBV** EBNA1 IgG^{+} **EBV** EBNA1 IgM^{+}	Anomalous reactivation	MBP13-32 MBP83-99 hMOG35-55 [Patient 11(21)]
DR15 04/15 Healthy (donor for DR15 HI mice)	F	28	NA	None	NA	NA	NA	NA	**JC** NA **EBV** VCA IgG^{+} **EBV** VCA IgM^{-} **EBV** VCA IgA^{-} **EBV** EA IgG^{+} **EBV** EBNA1 IgG^{+} **EBV** EBNA1 IgM^{+}	Anomalous reactivation	None [Normal 1(21)]
DR15 RRMS (donor for DR15 MS2 mice)	F	47	10	Dimethyl Fumarate Natalizumab (1 year and ongoing)	0/0 No relapses during the last year	(+) stable	(+) stable	1.5	**JC**$^{+}$ (0,96) **EBV** VCA IgG^{+} **EBV** VCA IgM^{-} **EBV** VCA IgA^{-} **EBV** EA IgG^{-}	Seropositive without symptoms of active infection	ND

									EBV EBNA1 IgG^{+} **EBV** EBNA1 IgM^{-}		
DR15 RRMS (donor for DR15 MS3 mice)	F	39	15	Interferon beta-1b Natalizumab (8 years and ongoing)	0/0 No relapse during the last year	(+) stable	(+) stable	2.0	**JC** (-) **EBV** VCA IgG^{+} **EBV** VCA IgM^{-} **EBV** VCA IgA^{+} **EBV** EA IgG^{+} **EBV** EBNA1 IgG^{+} **EBV** EBNA1 IgM^{-}	Suspect recent or ongoing reactivation	ND
DR15 RRMS (donor for DR15 MS4 mice)	F	53	23	Interferon beta-1a Interferon beta-1b Glatiramer Acetate Natalizumab (13 years and ongoing)	0/0 No relapse during the last year	(+) stable	(+) stable	3.5	**JC** (-) **EBV** VCA IgG^{+} **EBV** VCA IgM^{-} **EBV** VCA IgA^{-} **EBV** EA IgG^{+} **EBV** EBNA1 IgG^{+} **EBV** EBNA1 IgM^{+}	Anomalous reactivation	ND
DR15 RRMS (donor for DR15 MS5 mice)	F	30	13	Interferon beta-1a Interferon beta-1b Fingolimod Natalizumab (8 years and ongoing)	0/0 No relapse during the last year	(+) stable	(+) stable	1.5	**JC** (-) **EBV** VCA IgG^{+} **EBV** VCA IgM^{+} **EBV** VCA IgA^{+} **EBV** EA IgG^{-} **EBV** EBNA1 IgG^{+} **EBV** EBNA1 IgM^{-}	Suspect recent or ongoing reactivation	ND

KEY: EBV, Epstein-Barr virus; EDSS, expanded disability status scale; G, gender; Gd, gadolinium-enhancing lesions; JC; John Cunningham virus; NA, not applicable; ND, not done; RRMS, relapse-remitting MS;

866
867 **Figure legends**
868
869 **Figure 1**
870 **Reconstitution of a human adaptive immune system in B2m-NOG mice engrafted with**
871 **PBMC from MS patient and healthy donors. (A)** Progressive engraftment of human (h) CD45+
872 leukocytes from donors in groups of B2m-NOG mice, non-immunized (left) and immunized
873 for EAE using a myelin peptide cocktail in repeat immunizations with 200 µg/each myelin
874 peptide (EAE experiment 1), or single immunization with 100 µg/each myelin peptide (EAE
875 experiment 2) (right), measured in peripheral blood samples taken at different time points,
876 and in spleen recovered at sacrifice 42 days' post-transplantation (dpt 42). **(B)** Proportions of
877 $hCD4^+$ and $hCD8^+$ T cells in blood $hCD45^+CD3^+$ T cells at different time points. **(C)** Proportions
878 of human immune cell subpopulations in spleens of immunized and non-immunized mice at
879 dpt 42 (see also Supplementary Table 3). **(D)** Proportions of interferon-γ-producing and IL-
880 17A-producing $CD4^+$ and $CD8^+$ (or $CD4^-$) T cells in splenocytes recovered from mice in the
881 different groups at dpt 42. **(E)** Antigen-specific T cell proliferation responses to the
882 immunizing antigens (mMOG35-55, hMOG35-55, MOG1-20, MBP83-99), anti-hCD3 (positive
883 control) and medium (unstimulated; US), in splenocytes recovered from non-immunized and
884 immunized DR13 MS PBMC humanized mice at dpt 42. Results are expressed as a cell division
885 index. **(F)** Draining lymphoid structures in inguinal fat of mice engrafted with DR13 MS and
886 DR15 MS PBMC and immunized with myelin peptides, recovered at dpt 42.
887 Immunohistochemistry revealed the presence of hCD45- and mCD45-positive leukocytes,
888 hCD4- and hCD8-positive T cells, and hCD20-positive B cells (latter only DR13 MS mice). All
889 results are depicted as mean ± SEM. Statistical significance is shown after pairwise
890 comparisons between groups using Student's t test (*$p \leq 0.05$, **$p \leq 0.01$, ***$p \leq 0.001$).
891
892 **Figure 2**
893 **Human T cells accumulate at brain borders in non-immunized DR15 MS and DR15 HI mice,**
894 **and form spontaneous parenchymal lesions in brain of DR15 MS mice**
895 Immunohistochemical analysis of the brain from non-immunized PBMC B2m-NOG mice
896 showing infiltration by human (h) and mouse (m) CD45-positive leukocytes, and hCD8-
897 positive T cells, in brain border and parenchymal regions (denoted in diagrams of brain and
898 brainstem **A**). **(B, C)** Accumulation of hCD45- and mCD45-positive leukocytes and hCD8-
899 positive T cells, together with local activation of Iba1-positive microglia and GFAP-positive
900 astrocytes, at border regions in the brains of DR15 HI and DR15 MS mice, specifically at
901 meninges close to the optic tract (B, arrowheads) and in the connective tissue of the
902 interventricular foramen joining the lateral and third ventricles (C, arrowheads). Scattered
903 hCD45-positive leukocytes and hCD8 T cells in brain parenchyma of DR15 MS mice (C, arrows).
904 **(D)** Counting of barrier-associated and parenchymal hCD8- and hCD4-positive T cells at
905 borders and in parenchyma of whole coronal sections of brain/ mm^2 of humanized mice. (**E)**
906 Ratios of hCD4/hCD8 T cells at borders and parenchyma of selected humanized mice. **(F)** Small
907 hCD45-positive immune cell lesion in brainstem of DR15 MS1 mice (see also diagram A). **(G)**
908 hCD45-positive immune cell lesions in grey matter of hippocampus (i, ii) and sub-
909 hippocampus/thalamus (iii), and white matter of optic chiasm **(H)** of DR15 MS3 mice. **(I, J)**
910 hCD45-positive immune cell lesions in grey matter of thalamus and hippocampus,
911 respectively, of DR15 MS5 mice. Scale bars 100 µm; x20 objective (B, C, F), 200µm; 10x
912 objective (G), 100µm; 40x objective (H, I, J). All results are depicted as mean ± SEM. Statistical

913 analysis was performed by pairwise comparisons between different groups of mice using
914 Student's t test.
915
916 **Figure 3**
917 **Human T cells infiltrate spinal cord white matter in non-immunized DR15 MS and DR15 HI**
918 **mice, and form grey matter lesions in DR15 MS mice**
919 Immunohistochemical analysis of spinal cord from non-immunized PBMC B2m-NOG mice
920 showing infiltration by human (h) CD3-positive T cells in the grey and white matter regions.
921 **(A)** Infiltrating hCD3-positive T cells were scattered individually throughout spinal cord grey
922 and white matter and formed small lesions in the white matter (WM) of both DR15 MS and
923 DR15 HI mice (lower panels, arrowheads), and grey matter lesions only in DR15 MS mice
924 (upper panels, arrowheads). The dotted lines mark the boundary between grey matter and
925 white matter. **(B)** Counting of parenchymal hCD3-positive T cell lesions (≥ 3 adjacent cells) in
926 grey and white matter in whole spinal cord sections from DR15 HI and DR15 MS mice. **(C)**
927 Semi-quantitative estimation of hCD3-positive T cells in GM and WM regions in whole spinal
928 cord sections compared at equivalent cord regions from DR15 HI and DR15 MS mice. **(D)**
929 Ratios of hCD4/hCD8 T cells at borders and parenchyma of DR15 HI and DR15 MS mice. **(E)**
930 Double immunofluorescence staining for hCD45-positive leukocytes (green, arrowheads) and
931 MBP-positive myelin (red), with DAPI counterstained nuclei (blue), in spinal cord WM of DR15
932 MS mice. Scale bars 100 µm; x20 objective (A, upper panels); x40 objective (A, lower panels).
933 All results are depicted as mean ± SEM. Statistical analysis was performed by pairwise
934 comparisons between different groups of mice using Student's t test.
935
936 **Figure 4**
937 **Immunization with myelin peptides increases hCD4 T cell infiltration of brain parenchyma**
938 **resulting in mixed hCD4/hCD8 T cell lesions in brain of DR15 MS and DR15 HI mice**
939 Immunohistochemical analysis of the brain from PBMC B2m-NOG mice immunized for EAE
940 showing infiltration by human (h) and mouse (m) CD45-positive leukocytes, hCD8- and hCD4-
941 positive T cells, and local activation of Iba1-positive microglia and GFAP-positive astrocytes,
942 in brain regions denoted in the diagram **(A)**. **(B)** Individual hCD45-positive leukocytes and
943 hCD8-positive T cells form small lesions in the optic tract (arrowhead) in immunized DR15 HI
944 mice. **(C)** Counting of border-associated and parenchymal hCD45-positive T cells in whole
945 coronal sections of brain from non-immunized and immunized DR15 HI and DR15 MS mice.
946 **(D)** Counting of barrier-associated and parenchymal hCD4- and hCD8-positive T cells in whole
947 coronal sections of brain from non-immunized and immunized DR13 MS, DR15 HI and DR15
948 MS mice. **(E)** Ratios of hCD4/hCD8 T cells at borders and parenchyma of non-immunized and
949 immunized DR15 HI and DR15 MS mice. **(F)** Prominent lesions in the corpus callosum white
950 matter of two of three DR15 MS1 mice (arrowheads), containing hCD45- and mCD45-positive
951 leukocytes, hCD4- and hCD8-positive T cells and locally activated Iba1-positive microglia. Inset
952 shows a serial section stained by Luxol fast blue showing absence of demyelination. **(G)**
953 Double immunofluorescence staining for hCD45-positive leukocytes (green, arrowheads) and
954 MBP-positive myelin (red), with DAPI counterstained nuclei (blue), in corpus callosum in
955 immunized DR15 MS1 mice, showing inflammatory lesion without demyelination. **(H)** Small
956 white matter lesion in DR15 MS2 mouse. **(I)** Prominent white and **(J)** grey matter lesions in
957 DR15 MS3 mice containing both hCD4 and hCD8 T cells in DR15 MS3 mice. **(K)** Small human
958 hCD45-positive immune cell lesion in sub-thalamic area of DR15 MS5 mice. **(L)** Correlation

959 analysis between numbers of hCD4 or hCD8 with number of hCD45 lesions in brain
960 parenchyma of combined immunized DR15 HI and DR15 MS1-5 mice.
961 Scale bars 100 µm; x20 objective (B,F); x40 objective (G,K). All results are depicted as mean ±
962 SEM. Statistical analysis was performed by pairwise comparisons between different groups of
963 mice using Student's t test.
964
965 **Figure 5**
966 **Immunization with myelin peptides increases hCD4 T cell infiltration of spinal cord white**
967 **matter in both DR15 MS and DR15 HI mice**
968 Immunohistochemical analysis of spinal cord from PBMC B2m-NOG mice immunized for EAE
969 showing infiltration by human (h) CD3-positive T cells in the grey and white matter regions.
970 **(A)** Infiltrating hCD3-positive T cells scattered throughout spinal cord grey and white matter
971 and forming small lesions in the white matter (WM) of both DR15 MS1 and DR15 HI mice
972 (lower panels, arrowheads) The dotted lines mark the boundary between grey matter and
973 white matter. **(B)** Semi-quantitative estimation of hCD3-positive T cells in whole spinal cord
974 sections from DR15 HI and DR15 MS mice. **(C)** Counting of hCD3-positive T cell lesions (≥ 3
975 adjacent cells) in grey (GM) and white matter (WM) in whole spinal cord sections from DR15
976 HI and DR15 MS1 mice. **(D)** Ratios of hCD4/hCD8 T cells in spinal cord parenchyma of non-
977 immunized and immunized DR15 HI and DR15 MS mice. **(E)** Double immunofluorescence
978 staining for hCD45-positive leukocytes (green, arrowheads) and MBP-positive myelin (red),
979 with DAPI counterstained nuclei (blue), in white matter (WM) of immunized DR15 MS spinal
980 cord. All results are depicted as mean ± SEM. Scale bars 100 µm; x40 objective (A). Statistical
981 analysis was performed by pairwise comparisons between different groups of mice using
982 Student's t test.

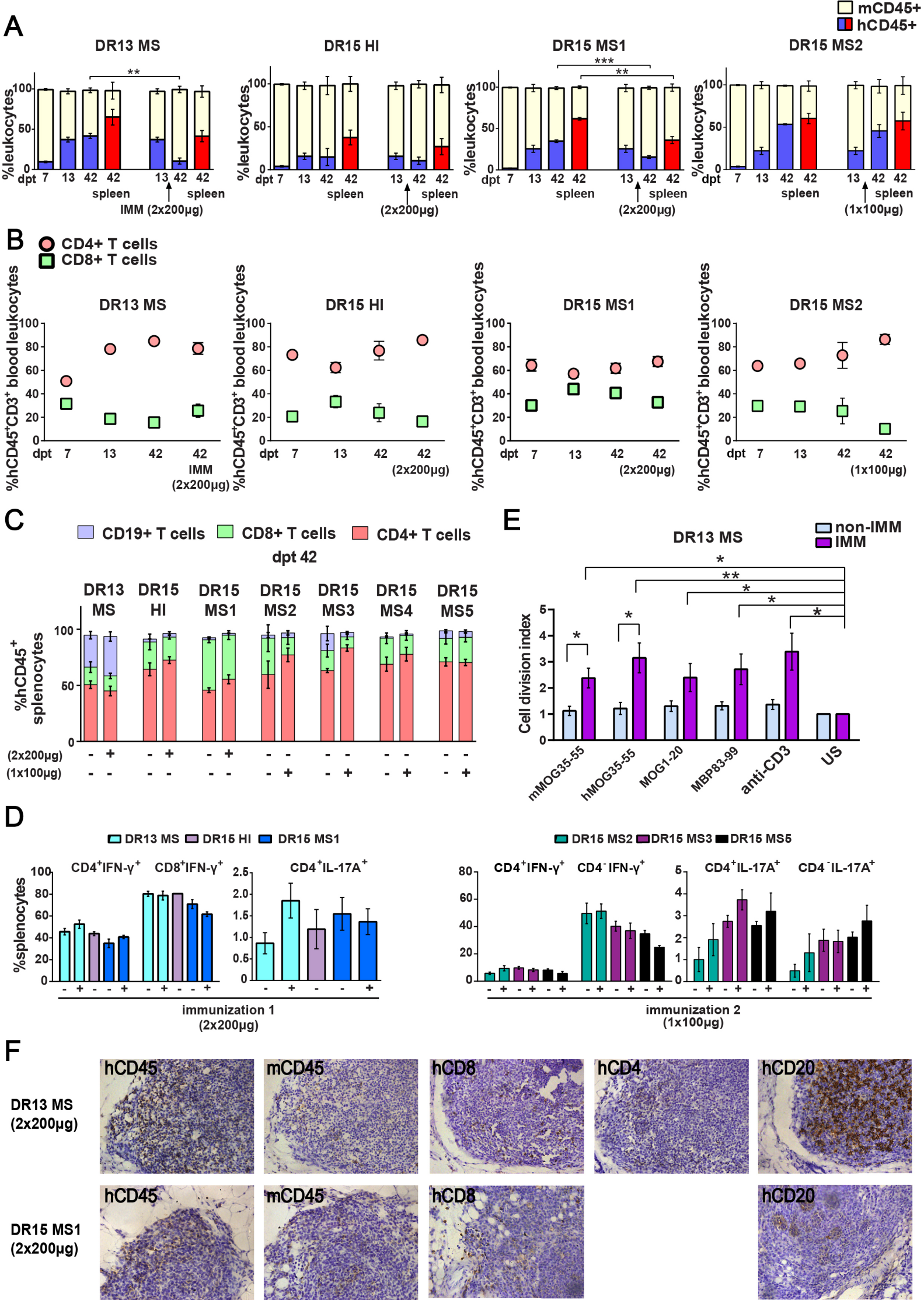
A
mCD45+
hCD45+
DR13 MS
DR15 HI
DR15 MS1
DR15 MS2
%leukocytes
dpt 7 13 42 42 13 42 42
spleen
IMM (2x200µg)
(2x200µg)
(1x100µg)
B
CD4+ T cells
CD8+ T cells
%hCD45+CD3+ blood leukocytes
dpt 7 13 42 42
IMM (2x200µg)
(2x200µg)
(1x100µg)
C
CD19+ T cells
CD8+ T cells
CD4+ T cells
dpt 42
DR13 MS
DR15 HI
DR15 MS1
DR15 MS2
DR15 MS3
DR15 MS4
DR15 MS5
%hCD45+ splenocytes
(2x200µg)
(1x100µg)
E
DR13 MS
non-IMM
IMM
Cell division index
mMOG35-55
hMOG35-55
MOG1-20
MBP83-99
anti-CD3
US
D
DR13 MS
DR15 HI
DR15 MS1
DR15 MS2
DR15 MS3
DR15 MS5
CD4+IFN-γ+
CD8+IFN-γ+
CD4+IL-17A+
CD4-IFN-γ+
CD4-IL-17A+
%splenocytes
immunization 1 (2x200µg)
immunization 2 (1x100µg)
F
DR13 MS (2x200µg)
DR15 MS1 (2x200µg)
hCD45
mCD45
hCD8
hCD4
hCD20

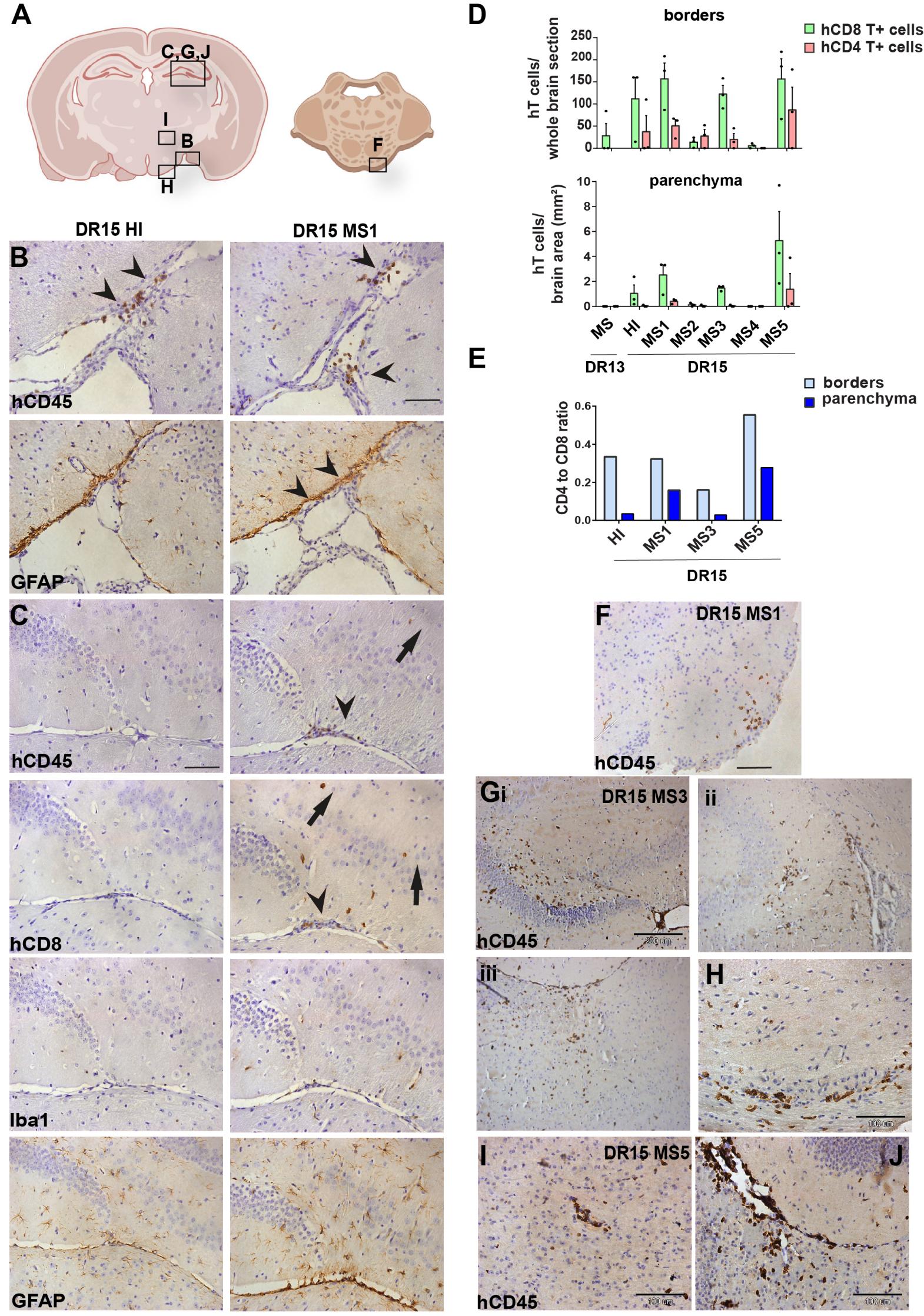
A
C,G,J
I
B
H
F
DR15 HI
DR15 MS1
B
hCD45
GFAP
C
hCD45
hCD8
Iba1
GFAP
D
borders
hCD8 T+ cells
hCD4 T+ cells
hT cells/ whole brain section
parenchyma
hT cells/ brain area (mm²)
MS
HI
MS1
MS2
MS3
MS4
MS5
DR13
DR15
E
borders
parenchyma
CD4 to CD8 ratio
HI
MS1
MS3
MS5
DR15
F
DR15 MS1
hCD45
Gi
DR15 MS3
ii
hCD45
iii
H
I
DR15 MS5
J
hCD45

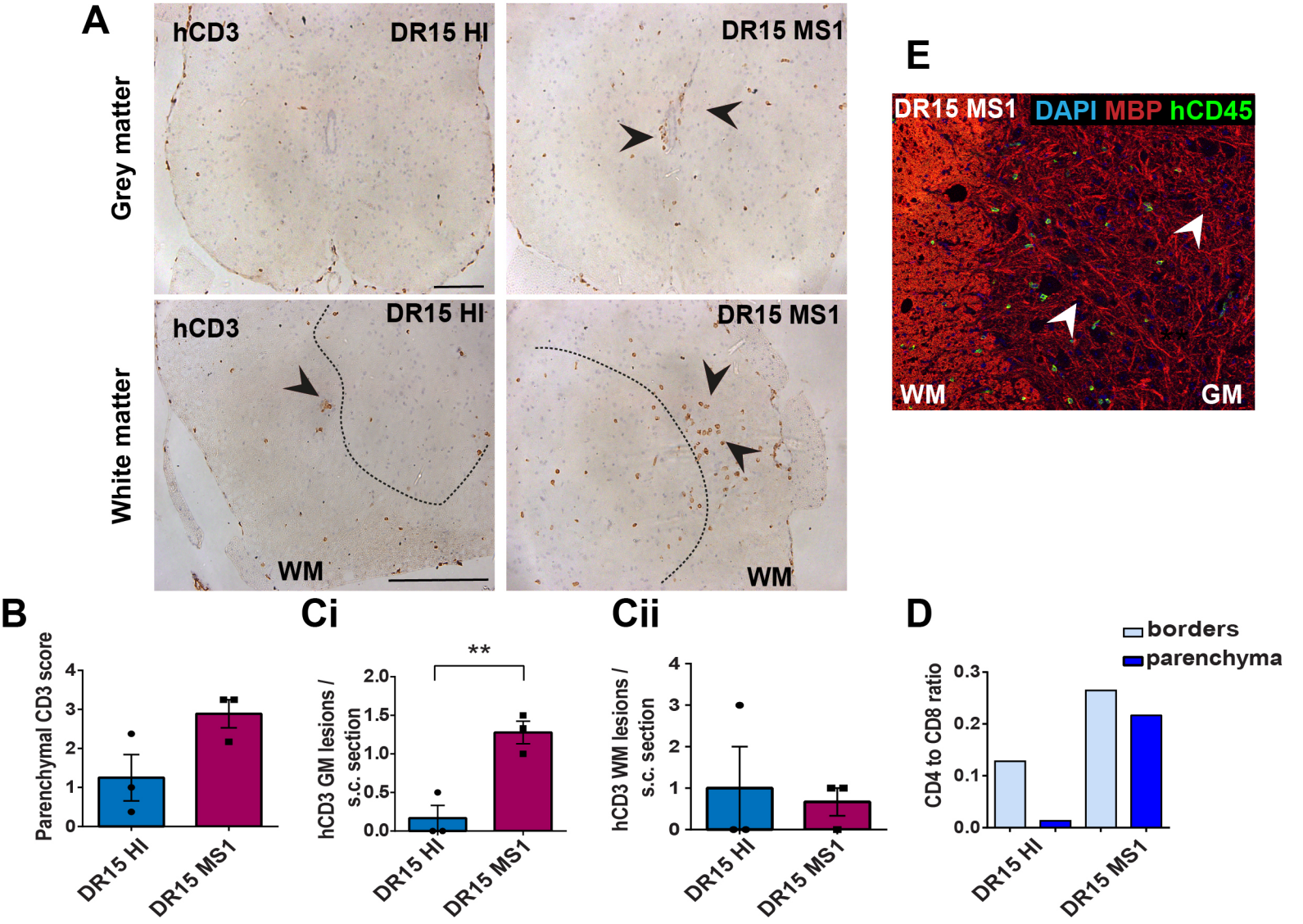
A
hCD3
DR15 HI
DR15 MS1
Grey matter
White matter
WM
E
DR15 MS1
DAPI MBP hCD45
WM
GM
B
Parenchymal CD3 score
DR15 HI
DR15 MS1
Ci
hCD3 GM lesions / s.c. section
**
Cii
hCD3 WM lesions / s.c. section
D
borders
parenchyma
CD4 to CD8 ratio

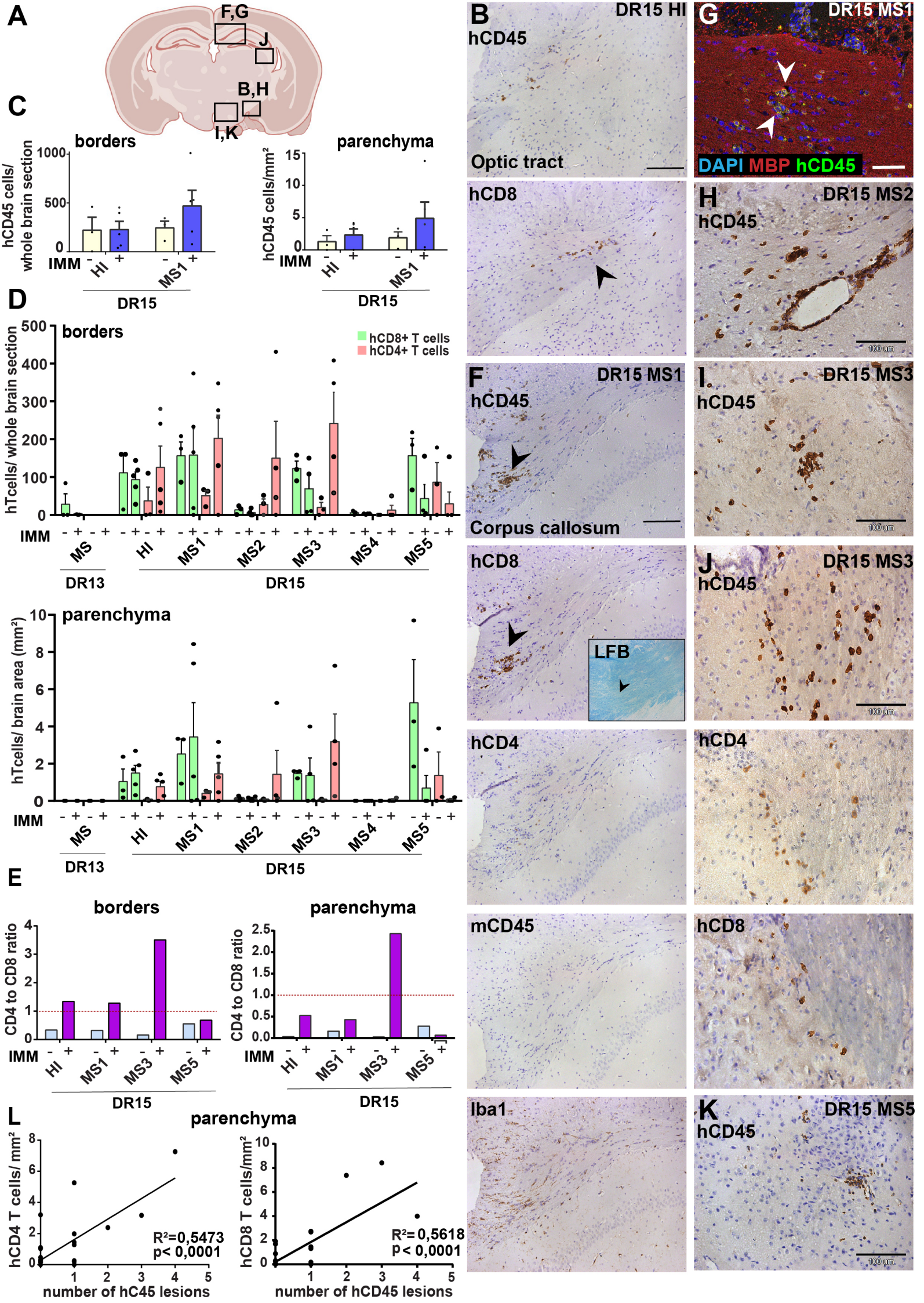
A
F,G
J
B,H
I,K
C
borders
parenchyma
hCD45 cells/ whole brain section
hCD45 cells/mm²
IMM
HI
MS1
DR15
D
borders
hCD8+ T cells
hCD4+ T cells
hTcells/ whole brain section
MS
HI
MS1
MS2
MS3
MS4
MS5
DR13
DR15
parenchyma
hTcells/ brain area (mm²)
E
borders
parenchyma
CD4 to CD8 ratio
L
parenchyma
hCD4 T cells/ mm²
hCD8 T cells/mm²
R²=0,5473
p< 0,0001
R²= 0,5618
p< 0,0001
number of hC45 lesions
number of hCD45 lesions
B
DR15 HI
hCD45
Optic tract
G
DR15 MS1
DAPI MBP hCD45
hCD8
H
DR15 MS2
hCD45
F
DR15 MS1
hCD45
Corpus callosum
I
DR15 MS3
hCD45
hCD8
LFB
J
DR15 MS3
hCD45
hCD4
hCD4
mCD45
hCD8
Iba1
K
DR15 MS5
hCD45

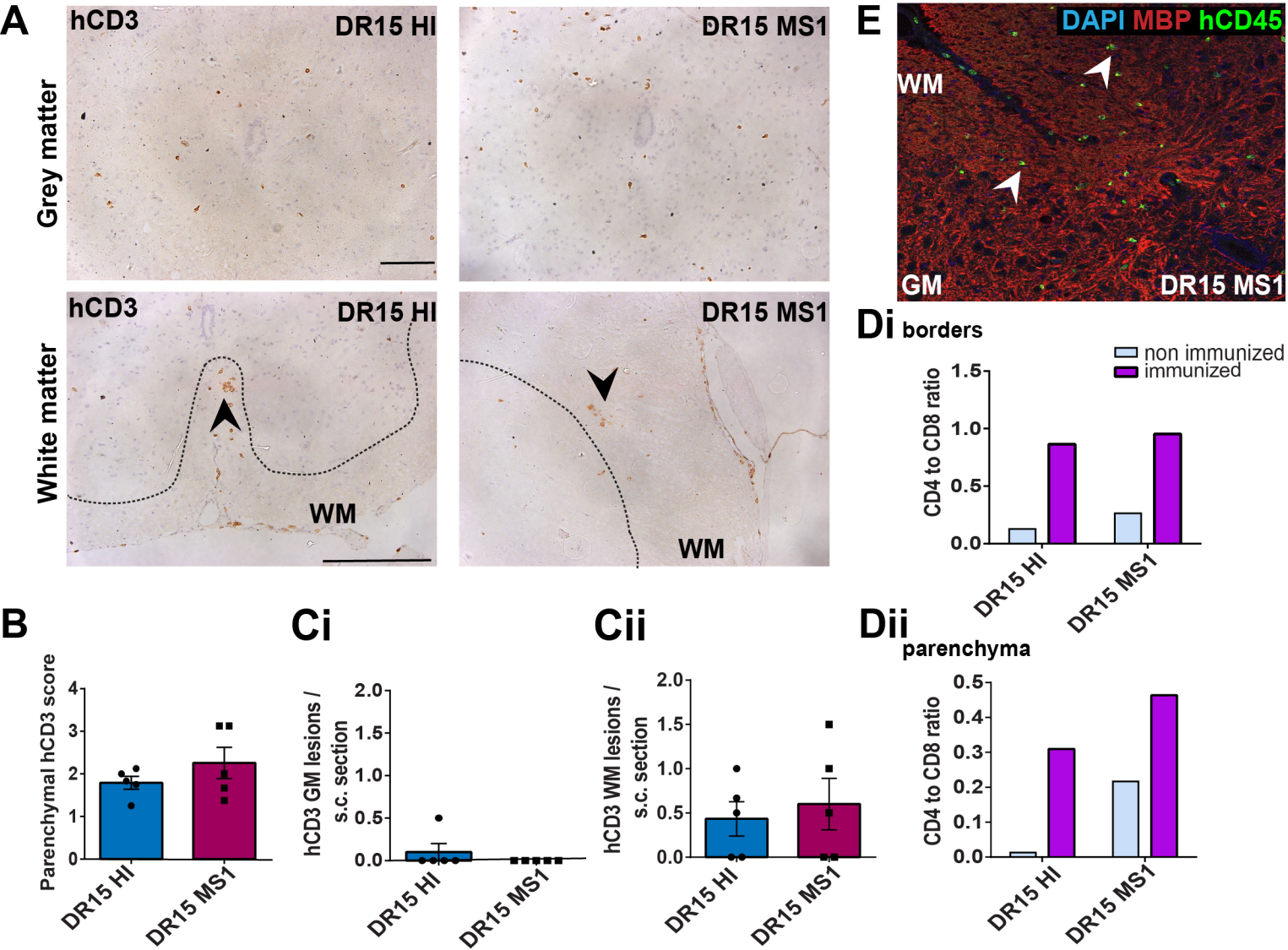
A
hCD3
DR15 HI
DR15 MS1
Grey matter
White matter
WM
E
DAPI MBP hCD45
GM
Di borders
non immunized
immunized
CD4 to CD8 ratio
B
Parenchymal hCD3 score
Ci
hCD3 GM lesions / s.c. section
Cii
hCD3 WM lesions / s.c. section
Dii parenchyma